HHS Public Access

Author manuscript

Cell Rep. Author manuscript; available in PMC 2020 June 18.

Published in final edited form as:

Cell Rep. 2020 April 14; 31(2): 107474. doi:10.1016/j.celrep.2020.03.038.

BCR-Induced Ca^{2+} Signals Dynamically Tune Survival, Metabolic Reprogramming, and Proliferation of Naive B Cells

Corbett T. Berry[1,2], **Xiaohong Liu**[1], **Arpita Myles**[3], **Satabdi Nandi**[4], **Youhai H. Chen**[3], **Uri Hershberg**[2,6], **Igor E. Brodsky**[1], **Michael P. Cancro**[3], **Christopher J. Lengner**[4,5], **Michael J. May**[4], **Bruce D. Freedman**[1,7,*]

[1]Department of Pathobiology, School of Veterinary Medicine, University of Pennsylvania, Philadelphia, PA 19104, USA

[2]School of Biomedical Engineering, Science and Health Systems, Drexel University, PA 19104, USA

[3]Department of Pathology and Laboratory Medicine, School of Medicine, University of Pennsylvania, Philadelphia, PA 19104, USA

[4]Department of Biomedical Sciences, School of Veterinary Medicine, University of Pennsylvania, Philadelphia, PA 19104, USA

[5]University of Pennsylvania Institute for Regenerative Medicine, Philadelphia, PA 19104, USA

[6]Department of Human Biology, Faculty of Sciences, University of Haifa, Haifa 3498838, Israel

[7]Lead Contact

SUMMARY

B cell receptor (BCR) engagement induces naive B cells to differentiate and perform critical immune-regulatory functions. Acquisition of functional specificity requires that a cell survive, enter the cell cycle, and proliferate. We establish that quantitatively distinct Ca^{2+} signals triggered by variations in the extent of BCR engagement dynamically regulate these transitions by controlling nuclear factor κB (NF-κB), NFAT, and mTORC1 activity. Weak BCR engagement induces apoptosis by failing to activate NF-κB-driven anti-apoptotic gene expression. Stronger signals that trigger more robust Ca^{2+} signals promote NF-κB-dependent survival and NFAT-, mTORC1-, and c-Myc-dependent cell-cycle entry and proliferation. Finally, we establish that CD40 or TLR9 costimulation circumvents these Ca^{2+}-regulated checkpoints of B cell activation and proliferation. As altered BCR signaling is linked to autoimmunity and B cell malignancies,

*Correspondence: bruce@vet.upenn.edu.

AUTHOR CONTRIBUTIONS

Conceptualization, C.T.B. and B.D.F.; Methodology, C.T.B. and B.D.F.; Investigation, C.T.B., X.L., A.M., S.N., and B.D.F.; Writing – Original Draft, C.T.B., M.J.M., and B.D.F.; Writing – Review & Editing, C.T.B, Y.H.C., I.E.B., M.P.C., C.J.L., and B.D.F.; Funding Acquisition, B.D.F. and M.J.M.; Resources, B.D.F., Y.H.C., I.E.B., M.P.C., C.J.L., and M.J.M.; Supervision, B.D.F.

SUPPLEMENTAL INFORMATION

Supplemental Information can be found online at https://doi.org/10.1016/j.celrep.2020.03.038.

DECLARATION OF INTERESTS

The authors declare no competing interests.

these results have important implications for understanding the pathogenesis of aberrant B cell activation and differentiation and therapeutic approaches to target these responses.

Graphical Abstract

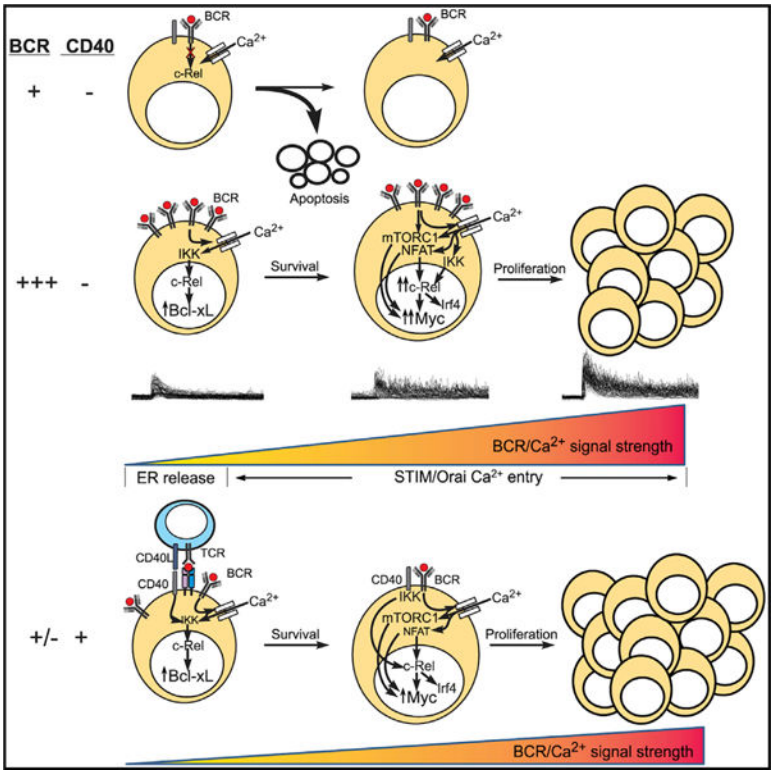

In Brief

Berry et al. establish that variations in the strength of BCR engagement are encoded as quantitatively distinct calcium signals that tune B cell fates by dynamically regulating NF-κB, NFAT, and mTORC1 activity. Targeting calcium signaling may thereby serve as an effective treatment strategy for regulating normal and pathological B cell activation.

INTRODUCTION

Quantitatively and qualitatively distinct signals generated by engagement of the B cell receptor (BCR) and costimulatory receptors on mature B cells control their survival, metabolic reprogramming, cell-cycle entry, and proliferation (Kouskoff et al., 1998; Casola et al., 2004; Pittner and Snow, 1998). Indeed, the mechanisms of BCR signal transduction have been extensively studied, yet relatively little is known about how differences in the affinity and avidity of BCR engagement are encoded within the cell and precisely how these signals are then decoded to regulate these key cell-fate transitions (Dal Porto et al., 2004; Kurosaki et al., 2010; Yam-Puc et al., 2018). Also unknown are the mechanisms by which costimulatory or co-activating signals impact the gain of BCR signaling to fine-tune a cell's fate. Previous efforts point to a relationship between the affinity and the avidity of antigen

binding to the BCR and the amplitude, duration, and periodicity of Ca^{2+} signals, and these studies reveal that distinct dynamics drive distinct fates of immature and mature B cells (Benschop et al., 1999; Hemon et al., 2017; Healy et al., 1997; Scharenberg et al., 2007; Nitschke et al., 1997; Cornall et al., 1998; Jellusova and Nitschke, 2012; Müller and Nitschke, 2014; Hoek et al., 2006). Indeed, mutations in signal transduction proteins downstream of the BCR, notably those that mobilize Ca^{2+}, can lead to altered B cell activation and differentiation, skewed humoral immune responses, autoimmune disease, and B cell malignancies (reviewed in Baba and Kurosaki, 2016). Thus, Ca^{2+} serves as a central molecular switch for encoding and transducing differences in BCR signaling with significant biological and pathological consequences.

Despite the well-established importance of Ca^{2+} in the antigen-induced responses of mature B cells, current understanding is also clouded by conflicting reports regarding the consequences of variations in BCR-induced Ca^{2+} signals. Findings from a recent study suggest that in the absence of costimulation, BCR-derived Ca^{2+} signals in mature B cells initiate mitochondrial dysfunction resulting in apoptosis (Akkaya et al., 2018). However, others have described a dose-dependent relationship between BCR signal strength and Ca^{2+} signals, cell survival, and proliferation (Matsumoto et al., 2011; Mao et al., 2016; Tang et al., 2017). Furthermore, the absolute role or requirement for Ca^{2+} seems to vary with the stage of mature B cell differentiation (Matsumoto et al., 2011). For example, in germinal center (GC) B cells, the coupling between the BCR and Ca^{2+} is disrupted, and these cells rely principally on costimulatory signals to drive class switch recombination and affinity maturation (Luo et al., 2018; Khalil et al., 2012). These costimulatory pathways, namely those triggered by CD40 and Toll-like receptor (TLR) engagement, are generally thought to be Ca^{2+} independent, suggesting that Ca^{2+}-dependent steps of B cell differentiation may be circumvented in some cases by costimulatory signals.

Among the mechanisms that critically regulate B cell activation and differentiation, several exhibit Ca^{2+} sensitivity. These include nuclear factor kB (NF-κB) (reviewed in Berry et al., 2018; Gerondakis and Siebenlist, 2010) and NFAT (Peng et al., 2001), which control the expression of diverse genes involved in cell survival and differentiation, mTORC1 (Li et al., 2016; Zhou et al., 2015), which regulates metabolic reprogramming, and c-Myc (Lindsten et al., 1988), which drives proliferative expansion (Stine et al., 2015; Saxton and Sabatini, 2017). In T cells, Ca^{2+} orchestrates a shift in cellular metabolism from oxidative phosphorylation to glycolysis by controlling the “master” regulators c-Myc and mTORC1 (Vaeth et al., 2017). However, the mechanisms by which the strength of antigen-receptor-induced quantitatively distinct Ca^{2+} signals tune steps that control B cell survival, metabolic reprogramming, cell-cycle entry, and proliferation are largely unexplored.

Consequently, we dissected the mechanisms by which Ca^{2+}, and specific properties of BCR-induced Ca^{2+} signals, regulate mature B cell survival, cell-cycle entry, and proliferation. We identified a relationship between the strength of BCR engagement and amplitude and periodicity of resulting Ca^{2+} signals. Further, we established how BCR-induced Ca^{2+} signals are decoded to regulate NF-κB-dependent steps of cell survival and mTORC1-and c-Myc-dependent cell-cycle entry and proliferation. Finally, we show how CD40 or TLR9 signaling can circumvent Ca^{2+}-regulated steps of B cell activation to promote enhanced survival and

proliferation. Importantly, given that enhanced or constitutive BCR signaling is linked to autoimmunity and B cell malignancies (Hemon et al., 2017), understanding these mechanisms that control early B cell differentiation has important implications for preventing aberrant B cell differentiation and developing therapeutics to modify the course of human disease.

RESULTS

Ca^{2+} Signals Encode BCR Signal Strength to Regulate B Cell Activation

The strength of antigen-induced signaling in B lymphocytes can be modulated by varying the concentration of agonist anti-BCR antibody (Stadanlick et al., 2008; Galibert et al., 1996; Hao and August, 2005). Indeed, progressive increases in BCR signal strength are encoded as quantitatively distinct intracellular Ca^{2+} signals (Figure 1A). Therefore, we varied BCR signal strength in this way to determine its relationship with Ca^{2+} and B cell activation, including survival, cell-cycle entry, and proliferation. The lowest signal strength (1 μg/mL anti-BCR) tested accentuated cell death relative to untreated cells (Figures 1B and 1C). Subsequent increases in BCR signal strength triggered a progressive increase in cell viability (Figures 1B and 1C), cell numbers (Figure 1D), the proportion of cells that divide (Figure 1E), and the number of divisions per cell (Figure 1F). The proportion of cells progressing beyond mid-G1 of the cell cycle, as indicated by Ki67 expression, also increased with BCR signal strength; although, at the highest anti-BCR concentration, only approximately half of B cells actively cycle at 36 h (Figure 1G). Collectively, these data indicate that the strength of BCR signaling dictates whether a B cell will live or die, the efficiency of cell-cycle entry, and the extent to which they proliferate.

Given that Ca^{2+} drives the expression of fate-specific genes (Healy et al., 1997, 1998; Dolmetsch et al., 1997; Matsumoto et al., 2011; Benschop et al., 1999), we implemented a genetic approach to examine the impact of variations in Ca^{2+} signal strength on BCR-induced gene expression. Specifically, we generated mice with a B-cell-specific (Mb1-Cre driven) deletion of *Stim1* and *Stim2* to preclude BCR-induced Orai-dependent Ca^{2+} entry. B cells from Stim1/Stim2 double-knockout (DKO) mice develop normally *in vivo* but exhibit defects in survival and proliferation *in vitro* (Matsumoto et al., 2011; Mao et al., 2016). Consistent with these previous reports, we observed a greater rate and extent of death of $Stim1^{fl/fl}Stim2^{fl/fl}Mb1^{cre+}$ (STIM DKO) by unstimulated B cells that was enhanced by BCR engagement (Figure 1H). Notably, most STIM DKO B cells died without proliferating (Figure 1I). Among the viable STIM DKO cells, relatively few entered the cell cycle (Figure 1J) and then divided only once (Figure 1I, STIM DKO, anti-BCR, lower right panel). Interestingly, this impairment in survival, cell-cycle entry, and proliferation by STIM DKO cells is comparable to the response of wild-type (WT) B cells to the lowest BCR strength tested, implying that a quantitative feature of Ca^{2+} signals, such as the initial peak amplitude, the steady-state concentration, or the frequency of spikes, tunes these responses to the BCR.

To better understand how Ca^{2+} regulates B cell fates, we quantified the impact of BCR signal strength on Ca^{2+} dynamics in mature WT and STIM DKO B cells. As anticipated, we observed a robust dose-dependent relationship between the strength of BCR engagement and

the pattern of Ca^{2+} signaling (Figure 1K). Specifically, the amplitude of the initial peak Ca^{2+} rise increased with BCR signal strength in both WT and STIM DKO cells, although the range was greatly attenuated in the absence of Ca^{2+} entry (Figure 1L). Furthermore, in WT cells, BCR strength also induced a dose-dependent increase in steady-state Ca^{2+} levels and spike frequency. By contrast, in STIM DKO cells, while higher concentrations of anti-BCR elicited a modest increase in spike frequency, Ca^{2+} levels rapidly decayed to pre-stimulation levels at all BCR strengths. Collectively, these results indicate that Ca^{2+} entry is needed to support sustained signaling and that quantitative properties of Ca^{2+} signals reflective of the strength of BCR engagement control B cell activation by regulating cell survival, cell-cycle entry, and proliferation.

STIM/Orai-Dependent Ca^{2+} Signals Drive Bcl-xL-Dependent Rescue from Apoptosis

We next focused on the mechanism by which BCR stimulation, and specifically Ca^{2+}, controls cell survival. Regardless of genotype or stimulus, nearly all nonviable B cells stained positive for Annexin V, suggesting that death of STIM DKO B cells occurs through apoptosis (Figure 2A). Indeed, a pan-caspase inhibitor (zVAD-fmk) attenuated caspase-3 cleavage and cell death (Figures 2B and 2C). Initiation of intrinsic apoptosis is dictated by a competitive equilibrium between Bcl-2 family members, including pro-apoptotic proteins and anti-apoptotic Bcl-2-like proteins (Enders et al., 2003). To evaluate whether Ca^{2+} acts to inhibit intrinsic apoptosis, we quantified its impact on the expression of four anti-apoptotic and seven pro-apoptotic genes. BCR stimulation of WT B cells led to a dramatic increase in the expression of anti-apoptotic genes *Bcl2la1* (encoding A1) and *Bcl2l1* (encoding Bcl-xL), and the induction of both genes was significantly attenuated in STIM DKO B cells (Figures 2D and S1A). Notably, BCR stimulation of WT B cells also led to a modest upregulation of several pro-apoptotic genes, including *Bak*, *Bax*, *Bbc3* (encoding Puma), *Bid*, *Bim*, and *Pmaip1* (encoding Noxa). Despite the observed apoptotic phenotype of STIM DKO B cells, upregulation of four of six pro-apoptotic genes was significantly decreased in the absence of Ca^{2+} entry. This result suggests the dominant impact of BCR-induced Ca^{2+} entry is to promote survival through anti-apoptotic gene expression. Indeed, BCR stimulation led to significant upregulation of Bcl-xL protein expression (Figure 2E), and the strength of BCR engagement correlated directly with the extent of its expression and viability of WT, but not DKO, cells (Figure 2F). Confirming that Bcl-xL induction by Ca^{2+} is sufficient to rescue B cells from apoptosis, heterologous Bcl-xL expression substantially improved cell survival in the absence of extracellular Ca^{2+} (Figure S1B). Thus, BCR-induced Ca^{2+} signals regulate cell survival by controlling the extent of Bcl-xL protein upregulation.

Apoptosis of primary B cells can also occur through extrinsic (death receptor) mechanisms that are initiated by ligation of receptors, including TNF-related apoptosis-inducing ligand (TRAIL), Fas, and tumor necrosis factor (TNF), linked to the activation of caspase-8 (Green and Llambi, 2015; Dickens et al., 2012). To evaluate whether BCR-induced Ca^{2+} signals also regulate extrinsic apoptosis, B cells were treated with the caspase 8 selective inhibitor z-IETD-fmk. Z-IETD-fmk did not rescue STIM DKO cells from BCR-induced apoptosis, indicating that cell-extrinsic apoptosis is unlikely to be involved in STIM DKO B cell death (Figure S1C). Importantly, although caspase-8 is a mediator of death-receptor-driven extrinsic apoptosis, it can also promote survival by preventing receptor-interacting serine/

threonine protein kinase-3 (Ripk3)-dependent necroptosis (Philip et al., 2016). Thus, to definitively assess the role of caspase-8, we evaluated the kinetics of *in vitro* survival of *Ripk3*$^{-/-}$ and *Ripk3*$^{-/-}$*Casp8*$^{-/-}$ B cells in the presence and absence of extracellular Ca^{2+}. Although the viability of *Rip3k*$^{-/-}$*Casp8*$^{-/-}$ B cells was marginally increased relative to WT cells in Ca^{2+}-depleted media, loss of caspase-8 and Rip3k did not restore Ca^{2+}-dependent survival (Figure S1D). Given that neither caspase-8 nor Rip3k expression impact Ca^{2+}-dependent rescue, we conclude that BCR-induced Ca^{2+} signals do not promote survival by antagonizing extrinsic apoptosis.

Ca^{2+}-Dependent Regulation of c-Rel Activation Promotes Bcl-xL Upregulation

To address how Ca^{2+} controls Bcl-xL expression, we focused on the NF-κB family member c-Rel because of its established role in BCR-induced *Bcl2l1* and *Bcl2la1* transcription (Sen, 2006; Hsia et al., 2002; Tumang et al., 1998; Grumont et al., 1998; Owyang et al., 2001). Consistent with a mechanistic link between Ca^{2+} and c-Rel activity, BCR-induced *Bcl2l1* (Figure 3A) and Bcl-xL (Figure 3B) expression and cell survival (Figure 3C) were similarly impaired in c-Rel KO and STIM DKO B cells. We next asked if BCR-induced Ca^{2+} signals control the activation of c-Rel, and we found that phosphorylation of IKKβ and its target, IκBα, and degradation of IκBα were inhibited in STIM DKO B cells (Figure 3D). Consistent with a block in IKK complex activation, both c-Rel and p65 nuclear localization were inhibited in STIM DKO B cells (Figure 3E), as was the expression of classical NF-κB target genes, including *Nfkbia* (encoding IκBα) and *Nfkb2* (encoding p100) (Figure 3F). Activation of preexisting p65 and c-Rel is critical during the initial phase of NF-κB-driven gene expression; however, *de novo* c-Rel induction is required to promote sustained NF-κB activity in lymphocytes (Venkataraman et al., 1995; Bajpai et al., 2000; Petro et al., 2000, 2002). Indeed, cells with higher c-Rel expression expressed more Bcl-xL (Pearson coefficient $\rho = 0.48$, $p = 0.0$; Figure 3G). Moreover, Ca^{2+} regulates *de novo* transcription of *Rel*, as this and c-Rel protein induction were restrained in STIM DKO B cells (Figures 3H and 3I).

We next asked how these two distinct waves of c-Rel activity (i.e., activation of pre-existing c-Rel and *de novo Rel* expression) are regulated. Previous studies indicate that activation of existing c-Rel is regulated by calcineurin (Cn)-dependent dephosphorylation of the CARD11-BCL-10-MALT1 (CBM) complex upstream of IKK activation (Frantz et al., 1994; Liu et al., 2016; Palkowitsch et al., 2011). However, various studies suggest that *de novo Rel* induction is controlled by both NFAT and NF-κB (Grumont et al., 2004; Nolz et al., 2007). Consistent with this model, we found that the Cn inhibitors cyclosporine A (CsA) and FK506 attenuated BCR-induced IκBα phosphorylation and degradation (Figure S2A), *Bcl2l1* mRNA (Figure S2B) and protein expression (Figure S2C), and B cell survival (Figure S2D). However, Cn also regulates NFAT activation and was required for c-Rel induction in B cells (Figure S2E). Consequently, we used IKKβ-deficient B cells to distinguish between the roles of NF-κB and NFAT in *de novo* c-Rel induction (Shaw et al., 1988; Flanagan et al., 1991). We found that c-Rel induction was comparable in WT and IKKβ knockout (KO) (isolated from *mb1-Cre* x *Ikk2*$^{fl/fl}$ mice) B cells and in both was attenuated by FK506 (Figure S2F). Together, these data establish that Ca^{2+} regulates c-Rel function by two distinct mechanisms. First, it controls IKK activity and the activation of

existing c-Rel to initiate expression of NF-κB target genes, including *Bcl2l1*. Second, it promotes Cn-induced, NFAT-dependent *de novo* c-Rel expression.

Ca^{2+}-Dependent mTORC1 Activation and Myc Expression Promotes Cell-Cycle Entry

In addition to its role in Bcl-xL expression and cell survival, c-Rel regulates cell-cycle entry by driving expression of proteins such as cyclin E and E2F3a (Cheng et al., 2003). However, entry into and progression through the cell cycle also requires a shift in cellular metabolism from oxidative phosphorylation to aerobic glycolysis (Pearce et al., 2013). We therefore asked if Ca^{2+} regulates key determinants of this metabolic reprogramming and proliferation, namely mechanistic target of rapamycin (mTOR) and c-Myc (Grumont et al., 2002; Wang et al., 2011; DeBerardinis et al., 2008; Newsholme et al., 1985). BCR engagement elicited phosphorylation of the mTORC1 target S6 (Figure 4A) and increased c-Myc expression (Figure 4B) in ~40% of WT cells but significantly fewer (~12%) STIM DKO B cells. Consistent with the established role for mTORC1 in c-Myc translation (Csibi et al., 2014), the induction of pS6 and c-Myc were highly correlated. Virtually all cells with high levels of pS6 express high levels of c-Myc (Figure 4C). Indeed, the mTORC1-specific inhibitor rapamycin and the pan-mTOR (mTORC1 and mTORC2) inhibitor Torin-1 both blocked BCR-induced c-Myc protein expression (Figure S3A). Furthermore, Ca^{2+} activation of mTORC1 is physiologically significant, as inhibition of mTORC1 and STIM deficiency similarly inhibited cell growth (Figures 4D and 4E), cell-cycle entry (Figure 4F), and proliferation (Figure 4G versus Figure 1).

Although Ca^{2+}-dependent regulation of mTORC1 likely impacts c-Myc translation, Ca^{2+} has been reported to drive *Myc* transcription (Vaeth et al., 2017; Lindsten et al., 1988; Nolz et al., 2007; Mognol et al., 2012). Indeed, BCR-induced *Myc* gene expression is attenuated in STIM DKO B cells (Figure 4H). Given that Cn/NFAT and c-Rel are known regulators of *Myc* expression, we next explored their roles in c-Myc induction using IKKβ KO and c-Rel KO mice (Grumont et al., 2002, 2004). Interestingly, we found that BCR-induced c-Myc induction is normal in IKKβ KO B cells but blocked by FK506 and removal of extracellular Ca^{2+} (Figure 4I). BCR-induced c-Myc expression is also significantly attenuated in c-Rel KO B cells (Figure S3B), indicating that both c-Rel and NFAT play primary and potentially redundant roles in c-Myc expression in mature B cells. Together, these results reveal that Ca^{2+} controls c-Myc expression by orchestrating its NFAT-and c-Rel-dependent transcription and mTORC1-regulated translation.

To address how Ca^{2+} regulates mTORC1 activity, we focused on Akt, which activates mTORC1 by inactivating the inhibitory TSC1-TSC2 complex (Inoki et al., 2002; Li et al., 2016; Divolis et al., 2016; Cao et al., 2017). Interestingly, BCR-induced Akt Thr308 and TSC2 Thr1462 phosphorylation with kinetics that corresponded to the phosphorylation of S6 (Figures 4J and 4K), and both TSC2 and S6 phosphorylation were transient in the absence of extracellular Ca^{2+}. Consistent with Akt mediating Ca^{2+} control of mTORC1 activity, we also examined Foxo1 localization, which is likewise regulated by Akt (Brunet et al., 1999). We found that BCR-induced Foxo1 export from the nucleus is attenuated in STIM DKO B cells (Figure S3C, left panels), WT B cells loaded with the intracellular Ca^{2+} chelator 1,2-bis-(2-aminophenoxy)ethane-N,N,N’,N’-tetraacetic acid tetra(acetoxymethyl) (BAPTA), and WT B

cells stimulated in Ca^{2+}-free medium (Figure S3C, right panels). Thus, Ca^{2+} dependent Akt activation coordinately controls both TSC2 phosphorylation and cytoplasmic localization of Foxo1.

Interestingly, despite the known role for Ca^{2+} in Akt activation (Divolis et al., 2016; Deb et al., 2004; Conus et al., 1998), we observed higher levels of BCR-induced Akt Thr308 phosphorylation under Ca^{2+}-free conditions than in the presence of Ca^{2+} (Figure 4J) and no relationship between Ca^{2+} and Akt Thr473 phosphorylation (Figure S3D). Furthermore, PDK1 (which phosphorylates Akt Thr308; Sarbassov et al., 2005; Shao et al., 2006) is constitutively phosphorylated and exhibited no sensitivity to BCR stimulation or Ca^{2+} (Figure 4J). Thus, while Ca^{2+} regulates Akt-dependent TSC2 phosphorylation, Akt Thr308 phosphorylation negatively correlates with mTORC1 activity, suggesting that Ca^{2+} control of mTORC1 is independent of Akt phosphorylation. We therefore asked if the Ca^{2+}-regulated proteins CaM and Cn, which interact with Akt and the mTORC1 complex (Ni et al., 2007; Li et al., 2016; Zhou et al., 2015; Vaeth et al., 2017), might regulate their activity. Indeed, the CaM inhibitor W7 and the Cn inhibitor FK506 both attenuated BCR-induced S6 phosphorylation (Figure S3E). As Cn activity is regulated by CaM binding, we conclude that Ca^{2+}-dependent control of mTORC1 in naive B cells is mediated by Cn-dependent regulation of Akt activity.

Ca^{2+} Signals Dynamically Tune mTORC1, NF-κB, and NFAT Activity

Given the relationship between the strength of BCR engagement and quantitative properties of Ca^{2+} dynamics (Figures 1K and 1L), we next asked if quantitative differences in BCR-induced Ca^{2+} signals might tune each of these key regulators of B cell activation. We began to dissect this relationship by examining the kinetics of Ca^{2+}-dependent S6K phosphorylation (pS6K). In WT B cells, phosphorylation of S6K was evident 30 min after stimulation and increased for at least 90 additional minutes (Figure 5A). By contrast, in STIM DKO B cells, BCR engagement induced a transient increase in pS6K that peaked at 60 min and then decayed. The transient activation of mTORC1 in STIM DKO cells suggests that mTORC1 activation may be sensitive to transient changes in cytoplasmic Ca^{2+} generated by endoplasmic reticulum (ER) release in the absence of Ca^{2+} entry (Figure 1K). To further examine if ER Ca^{2+} release is responsible for this transient mTORC1 activity in STIM DKO B cells, we loaded WT B cells with the high-affinity Ca^{2+} chelator BAPTA and then cultured these cells in Ca^{2+}-free medium. Under these conditions, BCR engagement failed to induce any detectable phosphorylation of S6 or S6K (Figure 5B). Further evidence that the amplitude and duration of BCR-induced changes in cytoplasmic Ca^{2+} directly tune mTORC1 activity is our observation that increasing the strength of BCR engagement produced a progressive and rapid increase in S6 phosphorylation (Figure 5C). Importantly, although muted relative to WT cells, the induction of pS6 in STIM DKO cells also exhibited a graded increase (Figure 1K, right panel) that parallels the graded impact of BCR signal strength on the extent of Ca^{2+} release from the ER in STIM DKO cells (see Figures 1K and 1L). Altogether, these results establish that mTORC1 activity is dynamically tuned by quantitative properties of BCR-induced Ca^{2+} signals and that the BCR-induced Ca^{2+} release from the ER can induce at least transient activation of mTORC1 in the absence of sustained Ca^{2+} entry through Orai channels.

We next sought to define the relationships among BCR signaling strength, Ca^{2+} dynamics (e.g., maximum peak, plateau, and spike frequency), and gene expression. To do this, we modulated the quantitative properties of intracellular Ca^{2+} signals by varying the extracellular [Ca^{2+}] at a fixed level (10 μg/mL anti-BCR) of BCR engagement (Figure 5D). This approach allowed us to distinguish between the impact of changing Ca^{2+} dynamics and confounding effects driven by other BCR-linked signaling pathways. We then examined the impact of these quantitatively distinct Ca^{2+} signals on the expression of NF-κB and NFAT target genes, including *Nfkbia*, *Irf4* (a previously described c-Rel target gene Grumont and Gerondakis, 2000), *Myc*, and *Rel*. For each of these genes (Figure 5E), we observed a direct relationship between extracellular Ca^{2+} and the level of expression. A graded increase in c-Myc, Irf4, and c-Rel protein was also observed when the BCR signal strength was varied at a fixed extracellular Ca^{2+} concentration, and like phosphorylation of S6, expression of each was muted at each signal strength in STIM DKO cells (Figure 5F). Together, these results establish a links among the strength of BCR engagement, quantitative properties of Ca^{2+} signals, and the pattern of NF-κB, NFAT, and mTORC1 activation. Furthermore, our results demonstrate that high-strength BCR signals can compensate to a limited extent for the absence of Ca^{2+} entry by modulating the amount of Ca^{2+} released from the ER.

Costimulatory Signals Bypass Ca^{2+} Signals to Promote Survival and Proliferation

Although BCR-induced Ca^{2+} signals drive cell survival, cell-cycle entry, and proliferation, under physiological conditions, these fates require licensing by co-activating signals. Among the best characterized is the CD40 ligand on T lymphocytes that cooperatively regulates B cell survival and proliferation during authentic immune responses (Luo et al., 2018). Therefore, we asked how CD40 signaling impacts the requirement for BCR-induced Ca^{2+} entry in cell survival and proliferation. Consistent with a previous study of STIM DKO B cells (Matsumoto et al., 2011), CD40 engagement alone or in conjunction with the BCR dramatically improved the viability of Mb1-cre^{+} and STIM DKO B cells (Figure 6A versus Figure 1H) by preventing caspase-3-mediated intrinsic apoptosis (Figures 6B and 6C). Furthermore, CD40 co-engagement dramatically increased cell growth (Figure 6D) and the proportion of STIM DKO B cells that proliferate relative to BCR stimulation alone (Figures 6E and 6F). Notably, CD40 co-engagement failed to fully rescue cell-cycle entry (Figure 6G) and proliferation of STIM DKO B cells (Figure 6H). Importantly, this rescue is independent of Ca^{2+}, as CD40 engagement has no impact on Ca^{2+} signaling dynamics (Figure S4A). Interestingly, stimulation with the TLR9 agonist CpG, which we previously found to mobilize cytoplasmic Ca^{2+} in B cells via scavenger-receptor-B1-mediated activation of TRPC3 channels (Zhu et al., 2009), also rescued WT and STIM DKO B cells from death (Figures S4B and S4C) and rescued STIM DKO cells from impaired proliferative expansion (Figures S4B and S4D). Thus, while alternative mechanisms of mobilizing Ca^{2+} could account for the ability of CpG to fully rescue defects in survival and proliferation of STIM DKO cells, CD40 costimulation bypasses the Ca^{2+}-dependent regulation of survival and proliferation (Zhu et al., 2009).

CD40-Dependent Canonical NF-κB Activation Rescues B Cells from Apoptosis

Given the established requirement for NF-κB in B cell survival, we next asked whether CD40-mediated rescue of STIM DKO B cells from apoptosis reflects its ability to bypass

Ca^{2+}-dependent steps of NF-κB activation. Indeed, CD40 and BCR co-engagement induced robust IKKβ and IκBα phosphorylation and IκBα degradation in STIM DKO B cells (Figure 7A). Furthermore, CD40 costimulation rescued p65 and c-Rel nuclear translocation (Figure 7B) and the expression of the NF-κB-dependent genes *Nfkbia* and *Nfkb2* (Figure 7C). While CD40 significantly increased *Bcl2l1* mRNA (Figure 7D) and Bcl-xL protein expression (Figure 7E), costimulation failed to fully rescue expression in STIM DKO B cells. Although CD40 activates both canonical and non-canonical NF-κB signaling (Coope et al., 2002), BLyS, which is a potent agonist of only non-canonical NF-κB (Stadanlick et al., 2008), improved the survival of unstimulated B cells but did not induce Bcl-xL expression (Figure 7E) or rescue viability of BCR-stimulated STIM DKO cells (Figure 7F). Thus, CD40-induced activation of canonical NF-κB is the primary mechanism by which CD40 rescues STIM DKO B cells from apoptosis, but CD40 costimulation fails to fully rescue *Bcl2l1* gene expression.

Ca^{2+} Entry Is Required for Efficient c-Rel-and NFAT-Dependent Gene Expression

Finally, we asked if the ability of CD40 to partially rescue cell-cycle entry and proliferation reflects its ability to bypass the requirement for Ca^{2+} in NFAT and mTORC1 activation and c-Rel expression. While CD40 drives robust IKK-dependent activation of preexisting c-Rel (Figure 7B), it did not efficiently rescue *de novo* c-Rel expression (Figure 7G) or the expression of the known anti-apoptotic and pro-proliferative c-Rel targets *Bcl21l*, *Bcl2la1*, *Myc*, *Ccne1* (encoding cyclin E), and *E2f3a* (encoding E2F3) (Figure 7H) in STIM DKO cells (Tumang et al., 1998). The level of c-Myc induction by antigen is especially critical, as it determines the kinetics and extent of lymphocyte proliferation (Heinzel et al., 2017). Notably, c-Myc protein expression was comparably lower in CD40 costimulated STIM DKO and c-Rel KO cells than in WT cells (Figure 7I), indicating that CD40 is unable to fully restore c-Rel-and NFAT-dependent steps of c-Myc expression despite its ability to increase TSC2 and S6 phosphorylation in the absence of Ca^{2+} (Figure 7J) and pS6 in STIM DKO B cells (Figure 7K).

DISCUSSION

The critical role of B cells in adaptive immunity reflects their capacity to produce antibodies that opsonize or neutralize pathogens and perform immune-regulatory functions. Although a repertoire of B cells with virtually infinite antigen specificity is generated during development, initial interactions of naive B cells with antigen and costimulatory ligands dictate cell fates and functions critical for appropriate and effective immunity. Foremost among the gaps in our understanding of these processes are (1) how variations in the affinity and avidity of antigen/antigen receptor interactions and costimulatory or coactivating signals are encoded and (2) how these signals are decoded at key developmental/differentiation stages.

Results herein establish that variations in the strength of BCR engagement are encoded as dynamic and quantitatively distinct fluctuations in the concentration of cytoplasmic Ca^{2+}. We find that the strength of BCR engagement is encoded in quantitative properties of intracellular Ca^{2+} signals, specifically their peak amplitude, steady-state concentration, and

spike frequency. Subsequently, these variations in Ca^{2+} dynamics control critical steps that regulate B cell survival, cell-cycle entry, and proliferation. Mechanistically, we found that BCR-induced STIM/Orai-dependent Ca^{2+} entry promotes cell survival by activating the IKK complex, thereby initiating c-Rel/p65 nuclear localization and the transcription of anti-apoptotic genes (i.e., *Bcl2l1* and *Bcl2la1*). Ca^{2+} entry also promotes Bcl-xL upregulation by increasing expression of c-Rel through NFAT-dependent transcription of *Rel*. ER release alone was insufficient to trigger IKK activation, c-Rel/p65 nuclear localization, *de novo Rel* expression, and NF-κB-dependent expression of *Bcl2l1* and *Bcl2la1*. However, CD40 stimulation or costimulation rescued STIM DKO B cells from apoptosis by activating the IKK complex. While not addressed directly here, CD40 has previously been shown to activate NF-κB signaling through TNF receptor-associated factor (TRAF)-dependent mechanisms (Jabara et al., 2002; Ahonen et al., 2002) and our data indicate that this occurs independently of intracellular Ca^{2+} signals.

We further demonstrated that Ca^{2+} orchestrates cell-cycle entry and proliferation via mechanisms distinct from those that control cell survival. Specifically, we found that Ca^{2+} tunes the activity of mTORC1 and c-Myc; both are reported to coordinate metabolic reprogramming required for cell-cycle entry and proliferation (Boothby and Rickert, 2017; Waters et al., 2018; Grumont et al., 2002; Vaeth et al., 2017). Optimal c-Myc expression required NFAT-and c-Rel-dependent *Myc* transcription and mTORC1-dependent Myc translation. Similarly, robust and persistent activation of mTORC1 required STIM/Orai-mediated Ca^{2+} entry, as ER release induced only transient mTORC1 activity. Loss of Ca^{2+} entry effectively decreases the strength of BCR signaling, but CD40 costimulation can circumvent the requirement for Ca^{2+} in NF-κB-and mTORC1-dependent steps of survival, cycle entry, and proliferation. Collectively, our data support a model in which the strength of BCR signaling is encoded in patterns of Ca^{2+} dynamics, which are decoded by varying the extent of NF-κB, NFAT, and mTORC1 activation.

Recent studies have identified a role for NFAT in B cell function and specifically demonstrated that STIM/Orai-dependent NFAT-driven gene expression regulates *Il10* induction by regulatory B cells to limit autoimmunity (Matsumoto et al., 2011; Tang et al., 2017). Here, we focused on the role for Ca^{2+} in NF-κB/c-Rel-dependent functions of B cells. While the general role of c-Rel-dependent gene expression in B cell survival, cell-cycle entry, and proliferation is established (Grumont et al., 1998; Tumang et al., 1998; Owyang et al., 2001; Hsia et al., 2002; Gilmore and Gerondakis, 2011; Cheng et al., 2003; Heise et al., 2014), we show that Ca^{2+} entry regulates c-Rel-dependent gene expression first by promoting IKK complex activation and then by driving NFAT-dependent *de novo Rel* transcription. Consistent with a direct functional link between Ca^{2+} entry and c-Rel is the similar impact of c-Rel and STIM deficiency on B cell viability and proliferative dynamics *in vitro*. This linkage reflects the requisite role for c-Rel in *Bcl2l1* and *Bcl2la1* expression and G1/S progression through its regulation of c-Myc, cyclin E, and E2f3 expression (Cheng et al., 2003; Grumont et al., 2002). Curiously, quantitative differences in c-Rel expression impacted the extent of c-Rel target gene expression, indicating that increases in c-Rel expression in the absence of adequate IKK complex activation may be sufficient to induce or maintain c-Rel target gene expression (Sen, 2006). Our finding that c-Myc expression is normal in IKKβ KO B cells supports this concept as c-Rel expression levels alone can

impact binding at the *Myc* promoter to regulate the efficiency of its induction (Duyao et al., 1990; Grumont et al., 2002). Interestingly, c-Rel KO mice exhibit defects in B cell development, germinal center maintenance, and antibody production (Heise et al., 2014; Gerondakis and Siebenlist, 2010; Gilmore and Gerondakis, 2011) that are not observed in STIM DKO mice (Matsumoto et al., 2011; Mao et al., 2016). Thus, the escape by STIM DKO B cells from these additional defects may reflect the ability of CD40 and TLR9 costimulation to bypass the Ca^{2+} requirement for c-Rel and p65 activation *in vivo*.

Our work also clarifies the role of Ca^{2+} entry in B cell apoptosis. Previous studies linked BCR-induced Ca^{2+} signals, in the absence of costimulation to mitochondrial dysfunction and cell death (Akkaya et al., 2018). In agreement, our data indicate that weak BCR signaling, induced with low concentrations of anti-BCR or by loss of STIM proteins, cause mitochondrial-dependent intrinsic apoptosis. However, our data also reveal that higher-strength BCR/Ca^{2+} signals induce sufficient expression of anti-apoptotic genes to prevent apoptosis. Furthermore, at low BCR/Ca^{2+} signal strengths, we find that CD40 signaling prevents mitochondrial-dependent apoptosis by activating the IKK complex. Thus, the extent of B cell survival is tuned by BCR signal strength and costimulatory signals.

A paradox highlighted by our results is that mice with a B-cell-specific deletion of *Stim1* and *Stim2* exhibit no apparent defect in antibody production despite decreased survival and proliferation potential *in vitro* (Matsumoto et al., 2011; Mao et al., 2016). During T-cell-dependent (TD) immune responses, T-cell-derived signals (CD40 ligand and cytokines) facilitate B cell expansion in germinal centers. The discrepancy between the *in vivo* and *in vitro* phenotypes could reflect maturation stage-specific requirements for BCR-induced Ca^{2+} signals or the presence of factors that bypass Ca^{2+}-dependent mechanisms of activation. Interestingly, germinal center B cells exhibit a cell-intrinsic block in BCR-induced Ca^{2+} signals (Khalil et al., 2012). This correlates with the reported inability of germinal center B cells to efficiently activate NF-κB, mTORC1, and c-Myc in response to BCR engagement (Luo et al., 2018). CD40 costimulation, acting independently of Ca^{2+}, likely compensates for this rewiring of BCR signaling to facilitate optimal NF-κB, mTORC1, and c-Myc activation (Luo et al., 2018). Thus, the capacity of CD40 to drive optimal signaling of both germinal center B cells and STIM DKO B cells represents a potential mechanism to circumvent the requirement for Ca^{2+} entry in TD antibody responses. During T-cell-independent (TI) immune responses, TI antigens induce antibody production without the help of T cells. TI antigens include type 1 (TI-1), which act as polyclonal B cell activators (e.g., CpG and lipopolysaccharide), and type 2 (TI-2), which are polysaccharides that directly crosslink the BCR (e.g., Ficoll) (Mond et al., 1995). Consistent with our *in vitro* TLR9 stimulation assays, TI-1 immune responses are normal in STIM DKO mice (Matsumoto et al., 2011; Mao et al., 2016). In contrast, TI-2 responses are BCR mediated and would be expected to be Ca^{2+}-entry dependent. However, TI-2 responses appear normal in STIM DKO mice. While not addressed here, TI-2 immune responses may require quantitatively smaller Ca^{2+} signals than those generated by STIM/Orai-mediated Ca^{2+} entry. Indeed, ablation of all three IP3 receptors (IP3R-TKO) and the attendant loss of BCR-induced ER release leads to decreased immunoglobulin M (IgM) antibody production in response to NP-Ficoll immunization (Tang et al., 2017). Additional studies are thus warranted to evaluate the cell-intrinsic role for Ca^{2+} release and entry in distinct B cell

lineages, including marginal zone B cells, which are the primary mediators of the TI-2 antibody response (Mond et al., 1995).

The notion that the strength of antigen receptor engagement is reflected in distinct patterns of Ca^{2+} signaling is not new. Seminal efforts more than 20 years ago established how NFAT and NF-κB are tuned to quantitative differences in antigen-receptor-induced Ca^{2+} signals (Dolmetsch et al., 1998; Healy et al., 1998; Li et al., 1998). Building upon this framework, we focused on developing a more comprehensive understanding of the mechanisms by which variations in Ca^{2+} signals, acting on NFAT, NF-κB, and mTORC1, regulate key steps of B cell activation (survival, cell-cycle entry, and proliferation). Furthermore, we determined how costimulatory signals, which can be generated by T cell help (CD40 ligand) or bacterial pathogen-associated molecular patterns (PAMPs) (e.g., CpG) to validate antigen authenticity, lower the BCR/Ca^{2+} threshold required to drive efficient B cell activation. It is our expectation that this new framework can be used to develop rational approaches for modulating diseases that reflect dysregulation of B cell survival and proliferation associated with immune-mediated disease and cancer.

STAR★METHODS

LEAD CONTACT AND MATERIALS AVAILABILITY

Further information and requests for resources and reagents should be directed to and will be fulfilled by the Lead Contact, Bruce D. Freedman (bruce@vet.upenn.edu). $STIM1^{fl/fl}$, $STIM2^{fl/fl}$, *Mb1*-cre single transgenic mice are available from Jackson Laboratories.

EXPERIMENTAL MODEL AND SUBJECT DETAILS

All animal studies were carried out in compliance with the guidelines of the Institutional Animal Care and Use Committee (IACUC) of the University of Pennsylvania and in accordance with the recommendations in the Guide and Use of Laboratory Animals of the National Institutes of Health. The animal protocol was approved by the IACUC of the University of Pennsylvania, Philadelphia, PA. C57BL/6 mice (WT) were obtained from the Jackson Laboratory. $Stim1^{fl/fl}$ and $Stim2^{fl/fl}$ mice (Oh-Hora et al., 2008) were a generous gift from Dr. Anjana Rao (UCSD). $Rel^{-/-}$ mice (Liou et al., 1999) were obtained from Dr. Hsiou-chi Liou. *Mb1*-cre mice (Hobeika et al., 2006) were obtained from Dr. Michael Atchison (University of Pennsylvania) and Dr. Montserrat Anguera (University of Pennsylvania). $Ikk2^{fl/fl}$ mice (Greten et al., 2004) were obtained from Dr. Michael Karen (UCSD). $Bcl2l1^{Tg}$ (Grillot et al., 1996) mice were obtained from Dr. Michael Cancro. 6-to 16 week old age and sex matched mice were used for all experiments.

METHOD DETAILS

Cell culture and stimulation—Naive splenic B cells were purified by positive selection using CD23 coated microbeads (Miltenyi Biotec, Bergisch Gladbach, Germany) followed by magnetic selection of labeled cells (B cell purity > 95%). All primary mouse B cells were cultured in RPMI 1640 medium (BioWhittaker, Walkersville, MD) supplemented with 10% fetal bovine serum (FBS, Hyclone, Thermoscientific, Logan, Utah), 2 mM L-glutamine, penicillin (50 U/ml), streptomycin (50 U/ml), pyruvate (1 mM), MEM NEAA (100 uM), 2-

ME (55 uM), HEPES (10 mM). For experiments in which B cells were stimulated in Ca^{2+} free media, 0.5 mM EGTA was added to complete RPMI media.-For *in vitro* stimulation assays, BCR was engaged using soluble 10 mg/mL anti-mouse F(ab′)2 antibody (Jackson ImmunoResearch, West Grove, PA) unless indicated otherwise. For CD40 engagement, LEAF purified anti-CD40 antibody (HM40–3, BioLegend, San Diego, CA) was used at a final concentration of 2 ug/mL. CpG (ODN1826: 5′-TCC ATG ACG TTC CTG ACG TT-3′) was synthesized and high-performance liquid chromatography purified by Integrated DNA Technologies (Coralville, IA). CpG was used at a final concentration of 1 μM. BLyS (R&D Systems, Minneapolis, MN) was used at final concentration of 100 ng/mL.

Flow Cytometry and FACS—Cell viability, cell size, and intracellular protein expression were measured by flow cytometry. For cell counting, 123count eBeads Counting Beads (Thermo Fisher) were used according to the manufacturer's instructions. For all flow cytometry experiments, cells were transferred to a round bottom 96 well plate, washed with FACS buffer (DPBS, 0.5% Bovine Serum Albumin, 2 mM EDTA), and stained with LIVE/DEAD Fixable Aqua Dead Cell Stain (L34957; Thermo Fisher) or LIVE/DEAD Fixable eF780 Dead Cell Stain (65–0865; Thermo Fisher) and Fc block (anti-CD16/32) prior to additional staining or fixation. Following additional processing (see below) cells were collected on an LSRFortessa or FACSCanto (BD Biosciences) and data were analyzed with FlowJo 9.9.6 software. Cells were gated on lymphocytes (by forward scatter (FSC-A) and side scatter (SSC-A), singlets (by FSC-W versus FSC-H and SSC-W versus SSC-H), and viability dye excluding cells. For analysis of *in vitro* stimulated B and T cells, cells were fixed with 4% PFA for 10 minutes followed by permeabilization with 1X Permeabilization Buffer (Thermo Scientific). Cells were stained overnight with antibodies to Myc PE (clone: D84C12, Cell Signaling), phospho-S6 PE-Cy7 (clone: D57.2.2E, Cell Signaling), c-Rel eF660 (clone: 1RE-LAH5, Thermo Scientific) or c-Rel PE (clone: REA397, Miltenyi Biotec), Irf4 PE-Vio770 (clone: REA201, Miltenyi Biotec), and/or Cleaved Caspase-3 (Asp175) (clone: 5A1E, Cell Signaling). For experiments with Bcl-xL, cells were stained for Bcl-xL (clone: 54H65, Cell Signaling) following by Alex Fluor 488 goat anti-rabbit secondary antibody (Thermo Fisher). For CFSE dilution assays, cells were washed 2X with DPBS before staining with 5 μM CFSE (Biolegend) for 6 minutes followed by the addition of FBS and 2 additional washes with complete RPMI. Labeled B cells were incubated for 72 hours in complete RPMI. CFSE dilution, viability, and cell counts were then assessed by flow cytometry. For AnnexinV apoptosis assays, cells were stained with L/D eF780 Viability dye and Annexin V FITC (Thermo Fisher) in binding buffer as described by the manufacturer.

Immunofluorescence analysis of c-Rel, p65, and Foxo1 localization—For immunofluorescence analysis, B cells were adhered to coverslips coated with Cell-Tak (BD Biosciences, Franklin Lakes, NJ) after stimulation. Cells were fixed with 4% paraformaldehyde for 10 minutes, permeabilized with 0.2% Triton X-100 for 5 minutes, treated with 5% BSA for 1 hour, stained with primary antibody O/N at 4C, and stained with secondary antibody at RT for 45 minutes. Nuclei were then labeled with Hoechst 33342 (Life Technologies, Cat #H3570, 4 μg/ml), washed 3 3 5 minutes in 1% BSA in PBS, and mounted in Fluoromount B (Fisher). Images of p65, c-Rel, and Foxo1 localization were

obtained with an inverted Leica SP5-II inverted (DMI6000 based) confocal microscope mounted on a Leica DMI4000 microscope (Leica Microsystems, Wetzlar, Germany) and imaging parameters were optimized independently for each channel to maintain fluorescence within the linear range while maximizing intensity resolution. Images analyzed using custom Macros in ImageJ to obtain nuclear intensities of p65, c-Rel, and Foxo1.

Immunoblot analysis—All cells were harvested and lysed using NP-40 lysis buffer consisting of 50 mM Tris-HCl (pH 7.5), 20mM EDTA, 1% NP-40 and complete inhibitors (1mM Sodium Orthovanadate, 1mM PMSF, 10 μg/ml Leupeptin, 5 μg/ml Aprotinin). Protein concentrations in cell lysates were determined using the Bio-Rad reagent (Bio-Rad Laboratories, Hercules, CA) and quantified in a Cary 50 Bio UV-visible Spectrophotometer. Proteins were resolved by SDS–polyacrylamide gel electrophoresis (4%–15%, Bio-Rad, Hercules, CA) then transferred onto polyvinylidene difluoride (PVDF) membranes (Millipore, Billerica, MA). Membranes were probed with respective primary anti-mouse antibodies including S6 Ribosomal Protein (54D2) Mouse mAb, Phospho-Tuberin/TSC2 (Thr1462) Antibody, Tuberin/TSC2 (D93F12) XP® Rabbit mAb #4308, Phospho-Akt (Thr308) (244F9) Rabbit mAb, Phospho-Akt (Ser473) (D9E) XP® Rabbit mAb, Akt (pan) (C67E7) Rabbit mAb, Phospho-PDK1 (Ser241) (C49H2) Rabbit mAb, Phospho-p70 S6 Kinase (Thr389) (108D2) Rabbit mAb, p70 S6 Kinase (49D7) Rabbit mAb, Phospho-IKKα/β (Ser176/180) (16A6) Rabbit mAb, IKKβ (D30C6) Rabbit mAb, IKKα, Phospho-IκBα (Ser32) (14D4) Rabbit mAb, anti-IκBα (L35A5) Mouse mAb, anti-alpha-tubulin, Tuberin/TSC2 (D93F12) XP® Rabbit mAb #4308. Blots were then incubated with Protein A HRP, anti-rabbit HRP, or anti-mouse HRP secondary antibodies (Thermo Fisher). Blots were developed with enhanced chemiluminescence using pierce ECL Western Blotting Substrate (Pierce, Rockford, IL). All immunoblots presented are from a single experiment representative of at least three independent experiments.

Quantitative Real-Time PCR (qRT-PCR)—cDNA was synthesized from RNA isolated (RNeasy Plus Micro Kit, QIAGEN) from cells with a high capacity cDNA reverse transcription kit (Applied Biosystems, Foster City, CA). cDNA was amplified with on a 6500 Fast Real-Time PCR System (Applied Biosciences, Warrington, United Kingdom) using Power SYBR Green PCR Master Mix (Applied Biosciences). Ct values were obtained in triplicate for each target including *Nfkbia, Nfkb2, Myc, Rel, Irf4, Bcl2l1, Bcl2l11, Bcl2a1, Bcl2, Mcl1, Bak1, Bax, Bad, Bbc3, Bid, Pmaimp1, Ccne1, E2f3*, Ubc, *and B2M* (See Table S1). Data were analyzed with the instrument software v1.3.1 (Applied Biosystems, Warrington, United Kingdom). All plots show relative expression based on difference between stimulated and unstimulated samples. For all plots mean ± 95% confidence interval is shown.

Calcium Imaging—Mouse B cells (5 million/mL) were loaded with 3 μM fura-2 acetoxymethyl ester (Molecular Probes, Eugene, OR) in external solution containing 145mM NaCl, 4.5mM KCl, 2mM $CaCl_2$, 1mM $MgCl_2$, 10mM glucose, 10mM HEPES, 2mM glutamine, and 2% fetal bovine serum (Hyclone, ThermoScientific, Logan, Utah) for 10 minutes at 25°C. Cells were adhered to coverslips coated with Cell-Tak (BD Biosciences, Franklin Lakes, NJ), mounted on the stage of a Leica DMI6000 microscope configured with

a Photometrics Evolve 512 Camera (Tucson, AZ) using an Olympus 40x oil objective (Shinjuku, Tokyo, Japan), and images were acquired with MetaFluor software (Molecular Devices, Downingtown, PA). The cells were then perfused with the balanced salt solution prior to addition of 10 μg/ml anti-IgM. Ca^{2+} mobilization was analyzed by plotting the emission ratio of 340/380-nm excitation for each cell. Each plot is the averaged ratio from at least 30 cells and is representative of at least 3 independent experiments. Analysis of Fura-2 ratios was completed in MATLAB (Mathworks, Massachusetts, USA) using custom written scripts. Maximum Fura-2 ratios were identified by calculating the maximum value within the first 5 minutes of recording and subtracting the average Fura-2 ratio from the first 0.5 minutes for each cell. The plateau value was measured by calculating the median Fura-2 ratio for each cell during the final 5 minutes of recording (10 min – 15 minutes). Spike interval number was calculated by detecting local minima and maxima and determined the absolute magnitude between the two local extrema. A fura-2 ratio "spike" threshold of 0.075 was identified as most accurate for spike detection. The total number of spikes were determined throughout the recording. Data visualization was performed using the statistical computing environment, R (v3.5.1), and RStudio (v1.1.456).

QUANTIFICATION AND STATISTICAL ANALYSIS

Significance for all statistical tests was determined at p values < 0.05 and is shown as * for $p < 0.05$, ** for $p < 0.01$, and *** for $p < 0.001$ in all figures except for qPCR data in which 95% confidence intervals were used. All data were assessed for normality using probability plots and the Kolmogorov-Smirnov test for normality. Normal distributions were compared using either two-tailed Student's t test or Welch's t test (depending on equality of variance) and non-normal data were compared using Wilcoxon rank sum test. The correlation between c-Rel and Bcl-xL expression was determined by calculating the Pearson correlation coefficient in WT anti-BCR stimulated samples. Unless otherwise indicated, results are representative of at least three independent experiments.

DATA AND CODE AVAILABILITY

This study did not generate/analyze relevant datasets.

Supplementary Material

Refer to Web version on PubMed Central for supplementary material.

ACKNOWLEDGMENTS

We thank Dr. Hsiou-chi Liou (Cornell University) for providing the $Rel^{-/-}$ mice, Dr. Michael Atchison (University of Pennsylvania) and Dr. Montserrat Anguera (University of Pennsylvania) for providing mb1-cre mice, and Dr. Michael Karin (UCSD) for providing $IKK2^{fl/fl}$ mice. We thank A.A.D., L.C., A.P., and M.C.A. for assisting with methodology and supplying valuable resources. These studies were funded by the NIH (grants R56AI125415 and RO1AI60921 to B.D.F., grants R01HL096642 and R01AR066567 to M.J.M., and AI128530 to I.E.B.).

REFERENCES

Ahonen C, Manning E, Erickson LD, O'Connor B, Lind EF, Pullen SS, Kehry MR, and Noelle RJ (2002). The CD40-TRAF6 axis controls affinity maturation and the generation of long-lived plasma cells. Nat. Immunol 3, 451–456. [PubMed: 11967542]

Akkaya M, Traba J, Roesler AS, Miozzo P, Akkaya B, Theall BP, Sohn H, Pena M, Smelkinson M, Kabat J, et al. (2018). Second signals rescue B cells from activation-induced mitochondrial dysfunction and death. Nat. Immunol 19, 871–884. [PubMed: 29988090]

Baba Y, and Kurosaki T (2016). Role of calcium signaling in B cell activation and biology. Curr. Top. Microbiol. Immunol 393, 143–174. [PubMed: 26369772]

Bajpai UD, Zhang K, Teutsch M, Sen R, and Wortis HH (2000). Bruton's tyrosine kinase links the B cell receptor to nuclear factor kappaB activation. J. Exp. Med 191, 1735–1744. [PubMed: 10811866]

Benschop RJ, Melamed D, Nemazee D, and Cambier JC (1999). Distinct signal thresholds for the unique antigen receptor-linked gene expression programs in mature and immature B cells. J. Exp. Med 190, 749–756. [PubMed: 10499913]

Berry CT, May MJ, and Freedman BD (2018). STIM-and Orai-mediated calcium entry controls NF-κB activity and function in lymphocytes. Cell Calcium 74, 131–143. [PubMed: 30048879]

Boothby M, and Rickert RC (2017). Metabolic regulation of the immune humoral response. Immunity 46, 743–755. [PubMed: 28514675]

Brunet A, Bonni A, Zigmond MJ, Lin MZ, Juo P, Hu LS, Anderson MJ, Arden KC, Blenis J, and Greenberg ME (1999). Akt promotes cell survival by phosphorylating and inhibiting a Forkhead transcription factor. Cell 96, 857–868. [PubMed: 10102273]

Cao Q, Yang Y, Zhong XZ, and Dong XP (2017). The lysosomal Ca^{2+} release channel TRPML1 regulates lysosome size by activating calmodulin. J. Biol. Chem 292, 8424–8435. [PubMed: 28360104]

Casola S, Otipoby KL, Alimzhanov M, Humme S, Uyttersprot N, Kutok JL, Carroll MC, and Rajewsky K (2004). B cell receptor signal strength determines B cell fate. Nat. Immunol 5, 317–327. [PubMed: 14758357]

Cheng S, Hsia CY, Leone G, and Liou HC (2003). Cyclin E and Bcl-xL cooperatively induce cell cycle progression in c-Rel−/−B cells. Oncogene 22, 8472–8486. [PubMed: 14627988]

Conus NM, Hemmings BA, and Pearson RB (1998). Differential regulation by calcium reveals distinct signaling requirements for the activation of Akt and p70S6k. J. Biol. Chem 273, 4776–4782. [PubMed: 9468542]

Coope HJ, Atkinson PG, Huhse B, Belich M, Janzen J, Holman MJ, Klaus GG, Johnston LH, and Ley SC (2002). CD40 regulates the processing of NF-kappaB2 p100 to p52. EMBO J 21, 5375–5385. [PubMed: 12374738]

Cornall RJ, Cyster JG, Hibbs ML, Dunn AR, Otipoby KL, Clark EA, and Goodnow CC (1998). Polygenic autoimmune traits: Lyn, CD22, and SHP-1 are limiting elements of a biochemical pathway regulating BCR signaling and selection. Immunity 8, 497–508. [PubMed: 9586639]

Csibi A, Lee G, Yoon SO, Tong H, Ilter D, Elia I, Fendt SM, Roberts TM, and Blenis J (2014). The mTORC1/S6K1 pathway regulates glutamine metabolism through the eIF4B-dependent control of c-Myc translation. Curr. Biol 24, 2274–2280. [PubMed: 25220053]

Dal Porto JM, Gauld SB, Merrell KT, Mills D, Pugh-Bernard AE, and Cambier J (2004). B cell antigen receptor signaling 101. Mol. Immunol 41, 599–613. [PubMed: 15219998]

Deb TB, Coticchia CM, and Dickson RB (2004). Calmodulin-mediated activation of Akt regulates survival of c-Myc-overexpressing mouse mammary carcinoma cells. J. Biol. Chem 279, 38903–38911. [PubMed: 15247222]

DeBerardinis RJ, Lum JJ, Hatzivassiliou G, and Thompson CB (2008). The biology of cancer: metabolic reprogramming fuels cell growth and proliferation. Cell Metab 7, 11–20. [PubMed: 18177721]

Dickens LS, Powley IR, Hughes MA, and MacFarlane M (2012). The 'complexities' of life and death: death receptor signalling platforms. Exp. Cell Res 318, 1269–1277. [PubMed: 22542855]

Divolis G, Mavroeidi P, Mavrofrydi O, and Papazafiri P (2016). Differential effects of calcium on PI3K-Akt and HIF-1a survival pathways. Cell Biol. Toxicol 32, 437–449. [PubMed: 27344565]

Dolmetsch RE, Lewis RS, Goodnow CC, and Healy JI (1997). Differential activation of transcription factors induced by Ca2+ response amplitude and duration. Nature 386, 855–858. [PubMed: 9126747]

Dolmetsch RE, Xu K, and Lewis RS (1998). Calcium oscillations increase the efficiency and specificity of gene expression. Nature 392, 933–936. [PubMed: 9582075]

Duyao MP, Buckler AJ, and Sonenshein GE (1990). Interaction of an NF-kappa B-like factor with a site upstream of the c-myc promoter. Proc. Natl. Acad. Sci. USA 87, 4727–4731. [PubMed: 2191300]

Enders A, Bouillet P, Puthalakath H, Xu Y, Tarlinton DM, and Strasser A (2003). Loss of the pro-apoptotic BH3-only Bcl-2 family member Bim inhibits BCR stimulation-induced apoptosis and deletion of autoreactive B cells. J. Exp. Med 198, 1119–1126. [PubMed: 14517273]

Flanagan WM, Corthésy B, Bram RJ, and Crabtree GR (1991). Nuclear association of a T-cell transcription factor blocked by FK-506 and cyclosporin A. Nature 352, 803–807. [PubMed: 1715516]

Frantz B, Nordby EC, Bren G, Steffan N, Paya CV, Kincaid RL, Tocci MJ, O'Keefe SJ, and O'Neill EA (1994). Calcineurin acts in synergy with PMA to inactivate I kappa B/MAD3, an inhibitor of NF-kappa B. EMBO J 13, 861–870. [PubMed: 8112299]

Galibert L, Burdin N, Barthélémy C, Meffre G, Durand I, Garcia E, Garrone P, Rousset F, Banchereau J, and Liu YJ (1996). Negative selection of human germinal center B cells by prolonged BCR cross-linking. J. Exp. Med 183, 2075–2085. [PubMed: 8642318]

Gerondakis S, and Siebenlist U (2010). Roles of the NF-kappaB pathway in lymphocyte development and function. Cold Spring Harb. Perspect. Biol 2, a000182. [PubMed: 20452952]

Gilmore TD, and Gerondakis S (2011). The c-Rel transcription factor in development and disease. Genes Cancer 2, 695–711. [PubMed: 22207895]

Green DR, and Llambi F (2015). Cell death signaling. Cold Spring Harb. Perspect. Biol 7, a006080. [PubMed: 26626938]

Greten FR, Eckmann L, Greten TF, Park JM, Li ZW, Egan LJ, Kagnoff MF, and Karin M (2004). IKKbeta links inflammation and tumorigenesis in a mouse model of colitis-associated cancer. Cell 118, 285–296. [PubMed: 15294155]

Grillot DA, Merino R, Pena JC, Fanslow WC, Finkelman FD, Thompson CB, and Nunez G (1996). bcl-x exhibits regulated expression during B cell development and activation and modulates lymphocyte survival in transgenic mice. J. Exp. Med 183, 381–391. [PubMed: 8627151]

Grumont RJ, Rourke IJ, O'Reilly LA, Strasser A, Miyake K, Sha W, and Gerondakis S (1998). B lymphocytes differentially use the Rel and nuclear factor kappaB1 (NF-kappaB1) transcription factors to regulate cell cycle progression and apoptosis in quiescent and mitogen-activated cells. J. Exp. Med 187, 663–674. [PubMed: 9480976]

Grumont RJ, Strasser A, and Gerondakis S (2002). B cell growth is controlled by phosphatidylinosotol 3-kinase-dependent induction of Rel/NF-kappaB regulated c-myc transcription. Mol. Cell 10, 1283–1294. [PubMed: 12504005]

Grumont RJ, and Gerondakis S (2000). Rel Induces Interferon Regulatory Factor 4 (IRF-4) Expression in Lymphocytes. J. Exp. Med 191, 1281–1292. [PubMed: 10770796]

Grumont R, Lock P, Mollinari M, Shannon FM, Moore A, and Gerondakis S (2004). The mitogen-induced increase in T cell size involves PKC and NFAT activation of Rel/NF-kappaB-dependent c-myc expression. Immunity 21, 19–30. [PubMed: 15345217]

Hao S, and August A (2005). Actin depolymerization transduces the strength of B-cell receptor stimulation. Mol. Biol. Cell 16, 2275–2284. [PubMed: 15728723]

Healy JI, Dolmetsch RE, Timmerman LA, Cyster JG, Thomas ML, Crabtree GR, Lewis RS, and Goodnow CC (1997). Different nuclear signals are activated by the B cell receptor during positive versus negative signaling. Immunity 6, 419–428. [PubMed: 9133421]

Healy JI, Dolmetsch RE, Lewis RS, and Goodnow CC (1998). Quantitative and qualitative control of antigen receptor signalling in tolerant B lymphocytes. Novartis Found. Symp 215, 137–144, discussion 144–145, 186–190. [PubMed: 9760576]

Heinzel S, Binh Giang T, Kan A, Marchingo JM, Lye BK, Corcoran LM, and Hodgkin PD (2017). A Myc-dependent division timer complements a cell-death timer to regulate T cell and B cell responses. Nat. Immunol 18, 96–103. [PubMed: 27820810]

Heise N, De Silva NS, Silva K, Carette A, Simonetti G, Pasparakis M, and Klein U (2014). Germinal center B cell maintenance and differentiation are controlled by distinct NF-κB transcription factor subunits. J. Exp. Med 211, 2103–2118. [PubMed: 25180063]

Hemon P, Renaudineau Y, Debant M, Le Goux N, Mukherjee S, Brooks W, and Mignen O (2017). Calcium signaling: from normal B cell development to tolerance breakdown and autoimmunity. Clin. Rev. Allergy Immunol 53, 141–165. [PubMed: 28500564]

Hobeika E, Thiemann S, Storch B, Jumaa H, Nielsen PJ, Pelanda R, and Reth M (2006). Testing gene function early in the B cell lineage in mb1-cre mice. Proc. Natl. Acad. Sci. USA 103, 13789–13794. [PubMed: 16940357]

Hoek KL, Antony P, Lowe J, Shinners N, Sarmah B, Wente SR, Wang D, Gerstein RM, and Khan WN (2006). Transitional B cell fate is associated with developmental stage-specific regulation of diacylglycerol and calcium signaling upon B cell receptor engagement. J. Immunol 177, 5405–5413. [PubMed: 17015726]

Hsia CY, Cheng S, Owyang AM, Dowdy SF, and Liou HC (2002). c-Rel regulation of the cell cycle in primary mouse B lymphocytes. Int. Immunol 14, 905–916. [PubMed: 12147627]

Inoki K, Li Y, Zhu T, Wu J, and Guan KL (2002). TSC2 is phosphorylated and inhibited by Akt and suppresses mTOR signalling. Nat. Cell Biol 4, 648–657. [PubMed: 12172553]

Jabara H, Laouini D, Tsitsikov E, Mizoguchi E, Bhan A, Castigli E, Dedeoglu F, Pivniouk V, Brodeur S, and Geha R (2002). The binding site for TRAF2 and TRAF3 but not for TRAF6 is essential for CD40-mediated immunoglobulin class switching. Immunity 17, 265–276. [PubMed: 12354380]

Jellusova J, and Nitschke L (2012). Regulation of B cell functions by the sialic acid-binding receptors siglec-G and CD22. Front. Immunol 2, 96. [PubMed: 22566885]

Khalil AM, Cambier JC, and Shlomchik MJ (2012). B cell receptor signal transduction in the GC is short-circuited by high phosphatase activity. Science 336, 1178–1181. [PubMed: 22555432]

Kouskoff V, Famiglietti S, Lacaud G, Lang P, Rider JE, Kay BK, Cambier JC, and Nemazee D (1998). Antigens varying in affinity for the B cell receptor induce differential B lymphocyte responses. J. Exp. Med 188, 1453–1464. [PubMed: 9782122]

Kurosaki T, Shinohara H, and Baba Y (2010). B cell signaling and fate decision. Annu. Rev. Immunol 28, 21–55. [PubMed: 19827951]

Li W, Llopis J, Whitney M, Zlokarnik G, and Tsien RY (1998). Cell-permeant caged InsP3 ester shows that Ca2+ spike frequency can optimize gene expression. Nature 392, 936–941. [PubMed: 9582076]

Li RJ, Xu J, Fu C, Zhang J, Zheng YG, Jia H, and Liu JO (2016). Regulation of mTORC1 by lysosomal calcium and calmodulin. eLife 5, e19360. [PubMed: 27787197]

Lindsten T, June CH, and Thompson CB (1988). Multiple mechanisms regulate c-myc gene expression during normal T cell activation. EMBO J 7, 2787–2794. [PubMed: 3053165]

Liou HC, Jin Z, Tumang J, Andjelic S, Smith KA, and Liou ML (1999). c-Rel is crucial for lymphocyte proliferation but dispensable for T cell effector function. Int. Immunol 11, 361–371. [PubMed: 10221648]

Liu X, Berry CT, Ruthel G, Madara JJ, MacGillivray K, Gray CM, Madge LA, McCorkell KA, Beiting DP, Hershberg U, et al. (2016). T cell receptor-induced nuclear factor kB (NF-κB) signaling and transcriptional activation are regulated by STIM1-and Orai1-mediated calcium entry. J. Biol. Chem 291, 8440–8452. [PubMed: 26826124]

Luo W, Weisel F, and Shlomchik MJ (2018). B cell receptor and CD40 signaling are rewired for synergistic induction of the c-Myc transcription factor in germinal center b cells. Immunity 48, 313–326.e5. [PubMed: 29396161]

Mao X, Zhang J, Han Y, Luan C, Hu Y, Hao Z, and Chen M (2016). Deficient for endoplasmic reticulum calcium sensors Stim1 and Stim2 affects aberrant antibody affinity maturation in B cells. Oncotarget 7, 60885–60895. [PubMed: 27572320]

Matsumoto M, Fujii Y, Baba A, Hikida M, Kurosaki T, and Baba Y (2011). The calcium sensors STIM1 and STIM2 control B cell regulatory function through interleukin-10 production. Immunity 34, 703–714. [PubMed: 21530328]

Mognol GP, de Araujo-Souza PS, Robbs BK, Teixeira LK, and Viola JP (2012). Transcriptional regulation of the c-Myc promoter by NFAT1 involves negative and positive NFAT-responsive elements. Cell Cycle 11, 1014–1028. [PubMed: 22333584]

Mond JJ, Lees A, and Snapper CM (1995). T cell-independent antigens type 2. Annu. Rev. Immunol 13, 655–692. [PubMed: 7612238]

Müller J, and Nitschke L (2014). The role of CD22 and Siglec-G in B-cell tolerance and autoimmune disease. Nat. Rev. Rheumatol 10, 422–428. [PubMed: 24763061]

Newsholme EA, Crabtree B, and Ardawi MS (1985). The role of high rates of glycolysis and glutamine utilization in rapidly dividing cells. Biosci. Rep 5, 393–400. [PubMed: 3896338]

Ni YG, Wang N, Cao DJ, Sachan N, Morris DJ, Gerard RD, Kuro-O M, Rothermel BA, and Hill JA (2007). FoxO transcription factors activate Akt and attenuate insulin signaling in heart by inhibiting protein phosphatases. Proc. Natl. Acad. Sci. USA 104, 20517–20522. [PubMed: 18077353]

Nitschke L, Carsetti R, Ocker B, Köhler G, and Lamers MC (1997). CD22 is a negative regulator of B-cell receptor signalling. Curr. Biol 7, 133–143. [PubMed: 9016707]

Nolz JC, Fernandez-Zapico ME, and Billadeau DD (2007). TCR/CD28-stimulated actin dynamics are required for NFAT1-mediated transcription of c-rel leading to CD28 response element activation. J. Immunol 179, 1104–1112. [PubMed: 17617603]

Oberst A, Dillon CP, Weinlich R, McCormick LL, Fitzgerald P, Pop C, Hakem R, Salvesen GS, and Green DR (2011). Catalytic activity of the caspase-8-FLIP(L) complex inhibits RIPK3-dependent necrosis. Nature 471, 363–367. [PubMed: 21368763]

Oh-Hora M, Yamashita M, Hogan PG, Sharma S, Lamperti E, Chung W, Prakriya M, Feske S, and Rao A (2008). Dual functions for the endoplasmic reticulum calcium sensors STIM1 and STIM2 in T cell activation and tolerance. Nat. Immunol 9, 432–443. [PubMed: 18327260]

Owyang AM, Tumang JR, Schram BR, Hsia CY, Behrens TW, Rothstein TL, and Liou HC (2001). c-Rel is required for the protection of B cells from antigen receptor-mediated, but not Fas-mediated, apoptosis. J. Immunol 167, 4948–4956. [PubMed: 11673501]

Palkowitsch L, Marienfeld U, Brunner C, Eitelhuber A, Krappmann D, and Marienfeld RB (2011). The Ca2+-dependent phosphatase calcineurin controls the formation of the Carma1-Bcl10-Malt1 complex during T cell receptor-induced NF-kappaB activation. J. Biol. Chem 286, 7522–7534. [PubMed: 21199863]

Pearce EL, Poffenberger MC, Chang CH, and Jones RG (2013). Fueling immunity: insights into metabolism and lymphocyte function. Science 342, 1242454. [PubMed: 24115444]

Peng SL, Gerth AJ, Ranger AM, and Glimcher LH (2001). NFATc1 and NFATc2 together control both T and B cell activation and differentiation. Immunity 14, 13–20. [PubMed: 11163226]

Petro JB, Rahman SM, Ballard DW, and Khan WN (2000). Bruton's tyrosine kinase is required for activation of IkappaB kinase and nuclear factor kappaB in response to B cell receptor engagement. J. Exp. Med 191, 1745–1754. [PubMed: 10811867]

Petro JB, Castro I, Lowe J, and Khan WN (2002). Bruton's tyrosine kinase targets NF-kappaB to the bcl-x promoter via a mechanism involving phospholipase C-gamma2 following B cell antigen receptor engagement. FEBS Lett 532, 57–60. [PubMed: 12459462]

Philip NH, DeLaney A, Peterson LW, Santos-Marrero M, Grier JT, Sun Y, Wynosky-Dolfi MA, Zwack EE, Hu B, Olsen TM, et al. (2016). Activity of uncleaved caspase-8 controls anti-bacterial immune defense and TLR-induced cytokine production independent of cell death. PLoS Pathog 12, e1005910. [PubMed: 27737018]

Pittner BT, and Snow EC (1998). Strength of signal through BCR determines the fate of cycling B cells by regulating the expression of the Bcl-2 family of survival proteins. Cell. Immunol 186, 55–62. [PubMed: 9637765]

Sarbassov DD, Guertin DA, Ali SM, and Sabatini DM (2005). Phosphorylation and regulation of Akt/PKB by the rictor-mTOR complex. Science 307, 1098–1101. [PubMed: 15718470]

Saxton RA, and Sabatini DM (2017). mTOR signaling in growth, metabolism, and disease. Cell 169, 361–371.

Scharenberg AM, Humphries LA, and Rawlings DJ (2007). Calcium signalling and cell-fate choice in B cells. Nat. Rev. Immunol 7, 778–789. [PubMed: 17853903]

Sen R (2006). Control of B lymphocyte apoptosis by the transcription factor NF-kappaB. Immunity 25, 871–883. [PubMed: 17174931]

Shao Z, Bhattacharya K, Hsich E, Park L, Walters B, Germann U, Wang YM, Kyriakis J, Mohanlal R, Kuida K, et al. (2006). c-Jun N-terminal kinases mediate reactivation of Akt and cardiomyocyte survival after hypoxic injury in vitro and in vivo. Circ. Res 98, 111–118. [PubMed: 16306447]

Shaw JP, Utz PJ, Durand DB, Toole JJ, Emmel EA, and Crabtree GR (1988). Identification of a putative regulator of early T cell activation genes. Science 241, 202–205. [PubMed: 3260404]

Stadanlick JE, Kaileh M, Karnell FG, Scholz JL, Miller JP, Quinn WJ 3rd, Brezski RJ, Treml LS, Jordan KA, Monroe JG, et al. (2008). Tonic B cell antigen receptor signals supply an NF-kappaB substrate for prosurvival BLyS signaling. Nat. Immunol 9, 1379–1387. [PubMed: 18978795]

Stine ZE, Walton ZE, Altman BJ, Hsieh AL, and Dang CV (2015). MYC, metabolism, and cancer. Cancer Discov 5, 1024–1039. [PubMed: 26382145]

Tang H, Wang H, Lin Q, Fan F, Zhang F, Peng X, Fang X, Liu J, and Ouyang K (2017). Loss of IP_3 receptor-mediated Ca^{2+} release in mouse B cells results in abnormal B cell development and function. J. Immunol 199, 570–580. [PubMed: 28615414]

Tumang JR, Owyang A, Andjelic S, Jin Z, Hardy RR, Liou ML, and Liou HC (1998). c-Rel is essential for B lymphocyte survival and cell cycle progression. Eur. J. Immunol 28, 4299–4312. [PubMed: 9862367]

Vaeth M, Maus M, Klein-Hessling S, Freinkman E, Yang J, Eckstein M, Cameron S, Turvey SE, Serfling E, Berberich-Siebelt F, et al. (2017). Store-operated Ca^{2+} entry controls clonal expansion of T cells through metabolic reprogramming. Immunity 47, 664–679.e6. [PubMed: 29030115]

Venkataraman L, Burakoff SJ, and Sen R (1995). FK506 inhibits antigen receptor-mediated induction of c-rel in B and T lymphoid cells. J. Exp. Med 181, 1091–1099. [PubMed: 7532676]

Wang R, Dillon CP, Shi LZ, Milasta S, Carter R, Finkelstein D, McCormick LL, Fitzgerald P, Chi H, Munger J, and Green DR (2011). The transcription factor Myc controls metabolic reprogramming upon T lymphocyte activation. Immunity 35, 871–882. [PubMed: 22195744]

Waters LR, Ahsan FM, Wolf DM, Shirihai O, and Teitell MA (2018). Initial B cell activation induces metabolic reprogramming and mitochondrial remodeling. iScience 5, 99–109. [PubMed: 30240649]

Yam-Puc JC, Zhang L, Zhang Y, and Toellner KM (2018). Role of B-cell receptors for B-cell development and antigen-induced differentiation. F1000Res 7, 429. [PubMed: 30090624]

Zhou X, Clister TL, Lowry PR, Seldin MM, Wong GW, and Zhang J (2015). Dynamic visualization of mTORC1 activity in living cells. Cell Rep 10, 1767–1777. [PubMed: 25772363]

Zhu P, Liu X, Treml LS, Cancro MP, and Freedman BD (2009). Mechanism and regulatory function of CpG signaling via scavenger receptor-B1 in primary B lymphocytes. J. Biol. Chem

Highlights

- BCR signal strength is encoded as quantitatively distinct intracellular Ca^{2+} signals
- Ca^{2+} dynamics are decoded by NF-κB, NFAT, and mTORC1 to drive cell fates
- BCR-induced Ca^{2+} signals are required for maximal B cell survival and proliferation
- CD40 compensates for weak BCR/Ca^{2+} signals to rescue NF-κB-and mTORC1-dependent fates

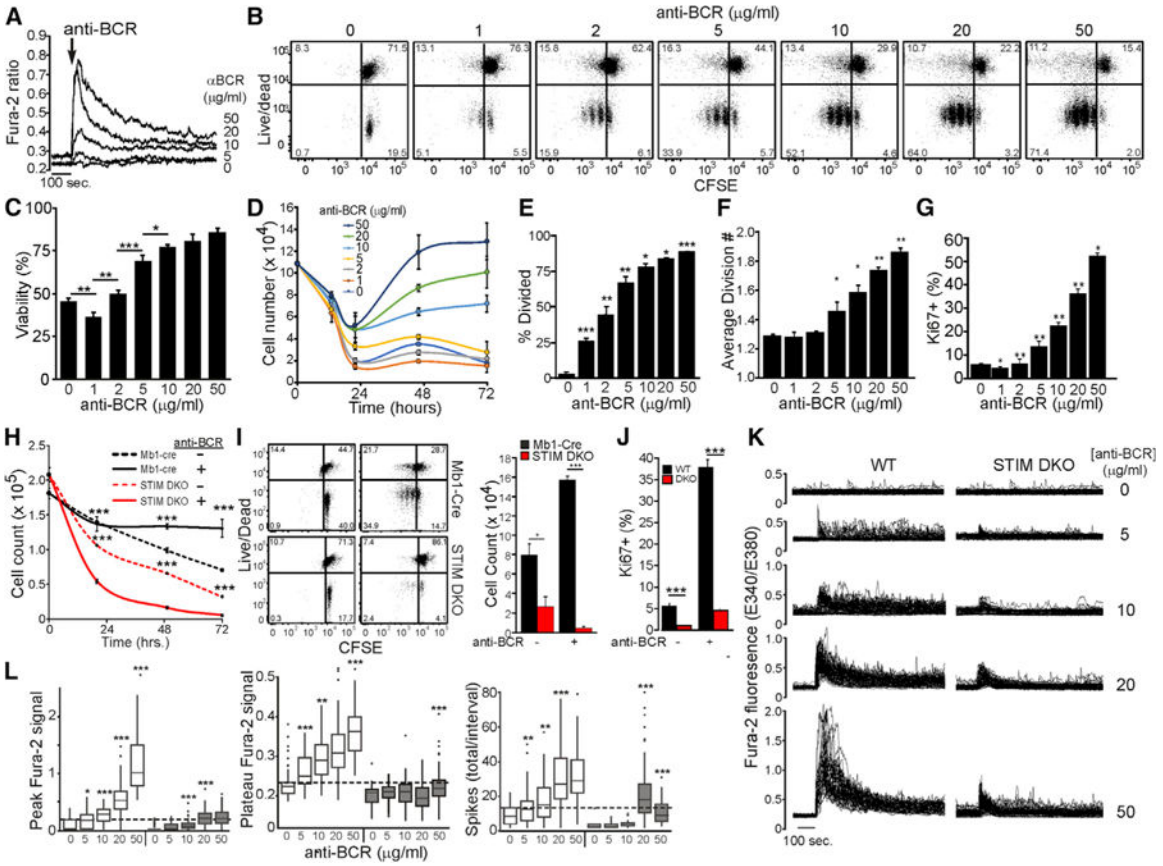

Figure 1. Ca^{2+} Signals Encode BCR Signal Strength to Regulate B Cell Activation

(A) Fura-2 ratiometric imaging of intracellular Ca^{2+} in WT $CD23^{+}$ B cells stimulated with anti-BCR as indicated. Average results are representative of three independent experiments with >50 cells per condition.

(B) CFSE-labeled WT $CD23^{+}$ B cells were stimulated in complete media with anti-BCR for 72 h as indicated. Carboxyfluorescein succinimidyl ester (CFSE) dilution and live/dead plots are representative of triplicate experiments.

(C and D) Viability of WT $CD23^{+}$ B cells as determined by the proportion of live/dead cells at 22 h (C) and total number of live cells at each initial anti-BCR concentration for each time point (D) (mean ± SD from triplicate wells).

(E and F) The proportion of divided cells (E) and average division number (F) for data shown in (B) (mean ± SD from triplicate wells).

(G) Ki67 expression in WT $CD23^{+}$ B cells stimulated for 32 h with anti-BCR as indicated (mean percentage ± SD from triplicate wells; statistical comparisons to adjacent [lower] concentration of anti-BCR).

(H) Total cell counts at indicated times are plotted for each condition (mean cell number ± SD of triplicate wells). CFSE-labeled $CD23^{+}$ B cells from $Stim1^{wt/}$ $wtStim2^{wt/wt}Mb1^{cre+}$ (Mb1-Cre) and $Stim1^{fl/fl}Stim2^{fl/fl}Mb1^{cre+}$ (STIM DKO) mice were unstimulated or stimulated for 72 h with anti-BCR. (I)C FSE dilution versus live/dead plot (left) is representative of results from triplicate wells (right) at 72 h.

(J) Ki67 expression (mean ± SD of triplicate wells) 32 h after anti-BCR stimulation of WT and STIM DKO B cells.
(K) Fura-2 ratiometric imaging of cytoplasmic [Ca^{2+}] in WT and STIM DKO B cells stimulated with anti-BCR as indicated. Each line depicts the response of a single cell.
(L) Boxplot representation of mean initial peak (upper left), average sustained concentration (between 10 and 15 min, upper right), and total spikes (lower left) in WT and STIM DKO B cells. Results are representative of three independent experiments with >50 cells per genotype/treatment, and statistical comparisons were made to adjacent (lower) concentration of anti-BCR. For all figures, *$p < 0.05$, **$p < 0.01$, ***$p < 0.001$.

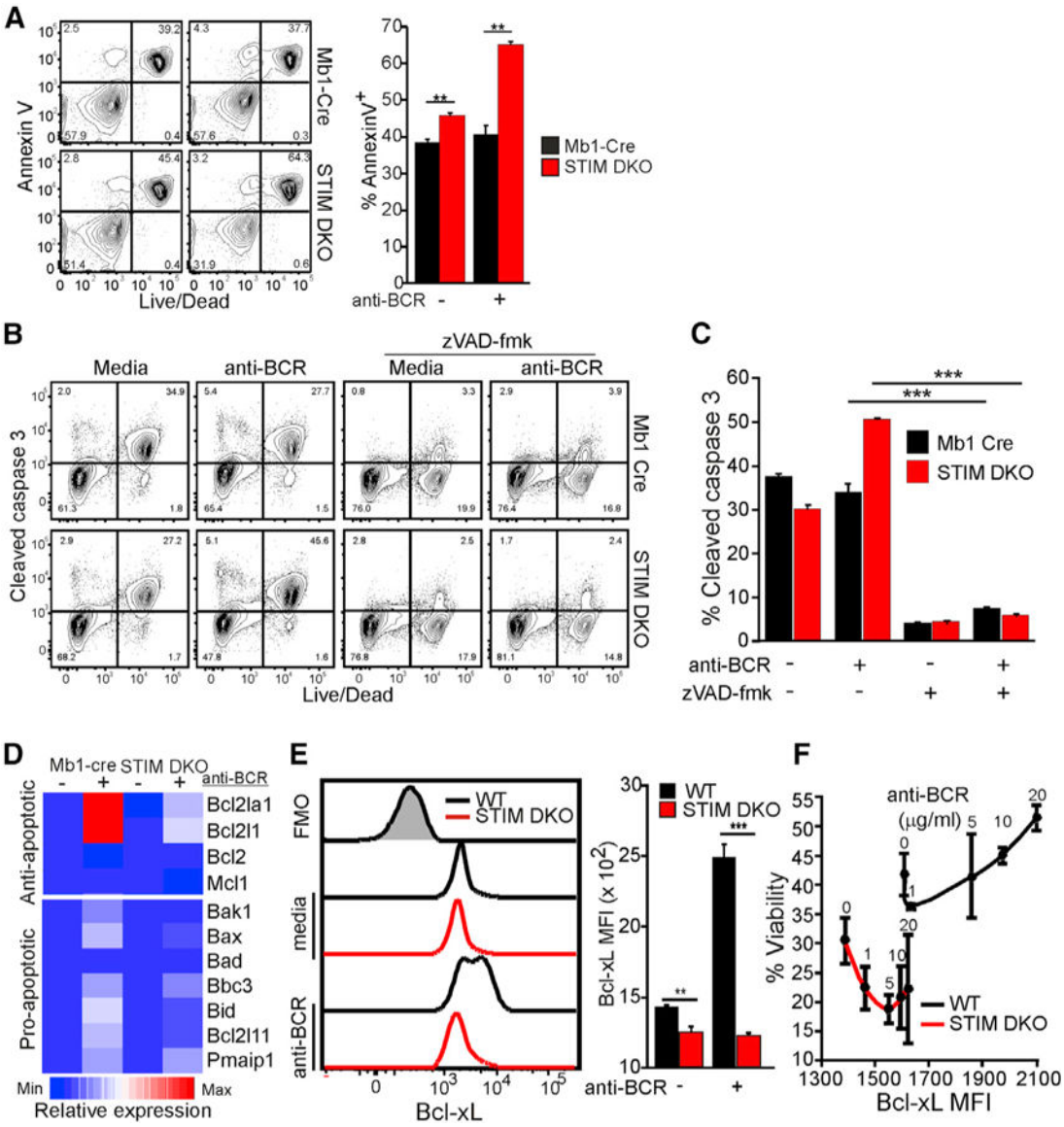

Figure 2. STIM/Orai-Dependent Ca^{2+} Signals Promote B Cell Survival through Induction of Bcl-xL Expression

WT and STIM DKO $CD23^{+}$ B cells were cultured in complete media in the absence or presence of anti-BCR.

(A) Annexin V and live/dead staining at 24 h of culture. (Left) Representative plot (right) and quantification of mean percentage of Annexin-V-stained cells (±SD from triplicate wells) are shown. (B and C) Flow cytometric analysis of intracellular cleaved caspase-3 at 12 h. The impact of the pan-caspase inhibitor zVAD-fmk (100 μM) on B cell viability was determined 12 h after anti-BCR stimulation.

(B) Representative cytometry plot (B) and percentage (mean ± SD) of cleaved caspase-3-stained cells from triplicate wells (C).

(D) Heatmap shows relative gene expression of anti-and pro-apoptotic genes based upon qRT-PCR analysis following culture as indicated for 6 h. Average expression from triplicate wells relative to Mb1-cre unstimulated (controls).

(E) Intracellular Bcl-xL expression (Fluorescence minus one (FMO), gray shaded histogram, left) in anti-BCR stimulated WT and STIM DKO B cells at 6 h (right, Bcl-xL MFI ± SD from triplicate wells).

(F) Bcl-xL mean fluorescence intensity (6 h) in $CD23^+$ B cells from WT (black line) and STIM DKO (red line) mice stimulated with anti-BCR (at indicated concentration) plotted versus viability (24 h, % live cells ± SD from triplicate wells and duplicate cultures). For all figures, *$p < 0.05$, **$p < 0.01$, ***$p < 0.001$.

See also Figure S1.

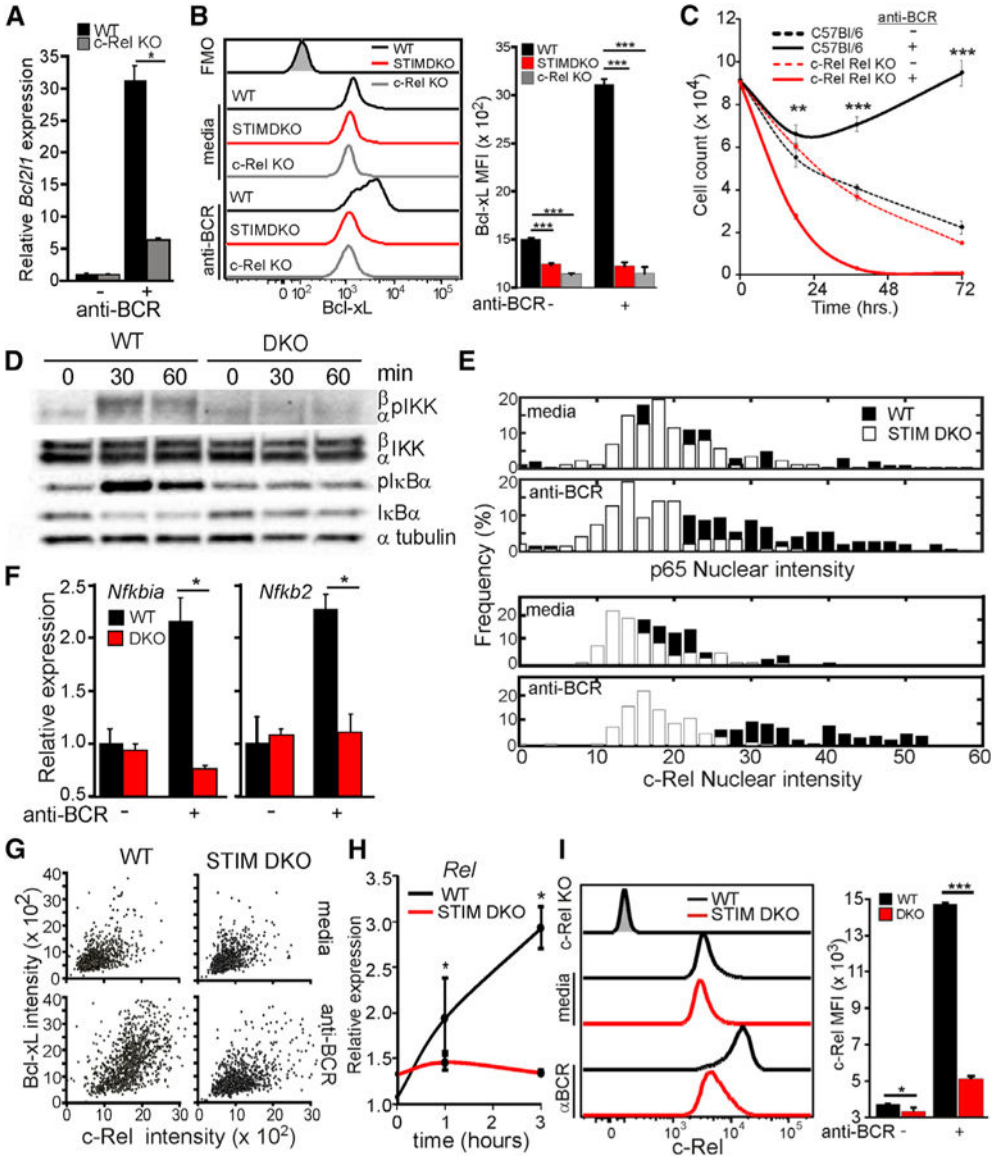

Figure 3. Ca^{2+} Entry Regulates NF-κB-Dependent Anti-apoptotic Gene Expression

(A) *Bcl2l1* expression after 6 h of anti-BCR stimulation in $CD23^+$ B cells from WT and c-Rel KO mice (mean ± 95% confidence interval; *, statistically significant).

(B) Intracellular Bcl-xL protein levels (relative to FMO, gray shaded histogram) in $CD23^+$ B cells from WT (black line), STIM DKO (gray line), and c-Rel KO (red line) mice 6 h after anti-BCR stimulation (left) and mean (median flourescence intensity (MFI) ± SD from triplicate wells) Bcl-xL fluorescence intensity (right).

(C) $CD23^+$ B cells from WT (solid line) and c-Rel KO (dashed line) mice were cultured for indicated times in media alone or media containing anti-BCR. The total number of live cells was enumerated, and mean cell number (±SD of triplicate wells) is plotted for the indicated time points.

(D) Immunoblot of anti-BCR-dependent NF-κB activation in $CD23^+$ WT and STIM DKO B cells at indicated time points.

(E) p65 (top) and c-Rel (bottom) nuclear localization in unstimulated (media) and anti-BCR stimulated (2 h) WT (black) and STIM DKO (white) B cells. Overlay of average c-Rel and p65 nuclear cell intensity (>70 cells per group) is shown.(F) *Nfkbia* (IκBα) and *Nfkb2* (p100) mRNA expression in $CD23^+$ B cells from WT and STIM DKO mice cultured for 3 h in the presence or absence of anti-BCR (mean ± 95% confidence interval; *, statistically significant).

(G) Scatterplot of c-Bcl-xL and Rel expression in individual WT (left) and STIM DKO (right) B cells cultured in the absence (media) and presence of anti-BCR for 20 h.

(H) Time course of anti-BCR-induced *Rel* expression in $CD23^+$ B cells from WT and STIM DKO mice (mean ± 95% confidence interval; *, statistically significant).

(I) c-Rel expression in WT (black line) and STIM DKO (red line) B cells cultured for 12 h with anti-BCR. (Left) Mean c-Rel MFI (±SD from triplicate wells, right). For all figures except where indicated, $*p < 0.05$, $**p < 0.01$, $***p < 0.001$. See also Figure S2.

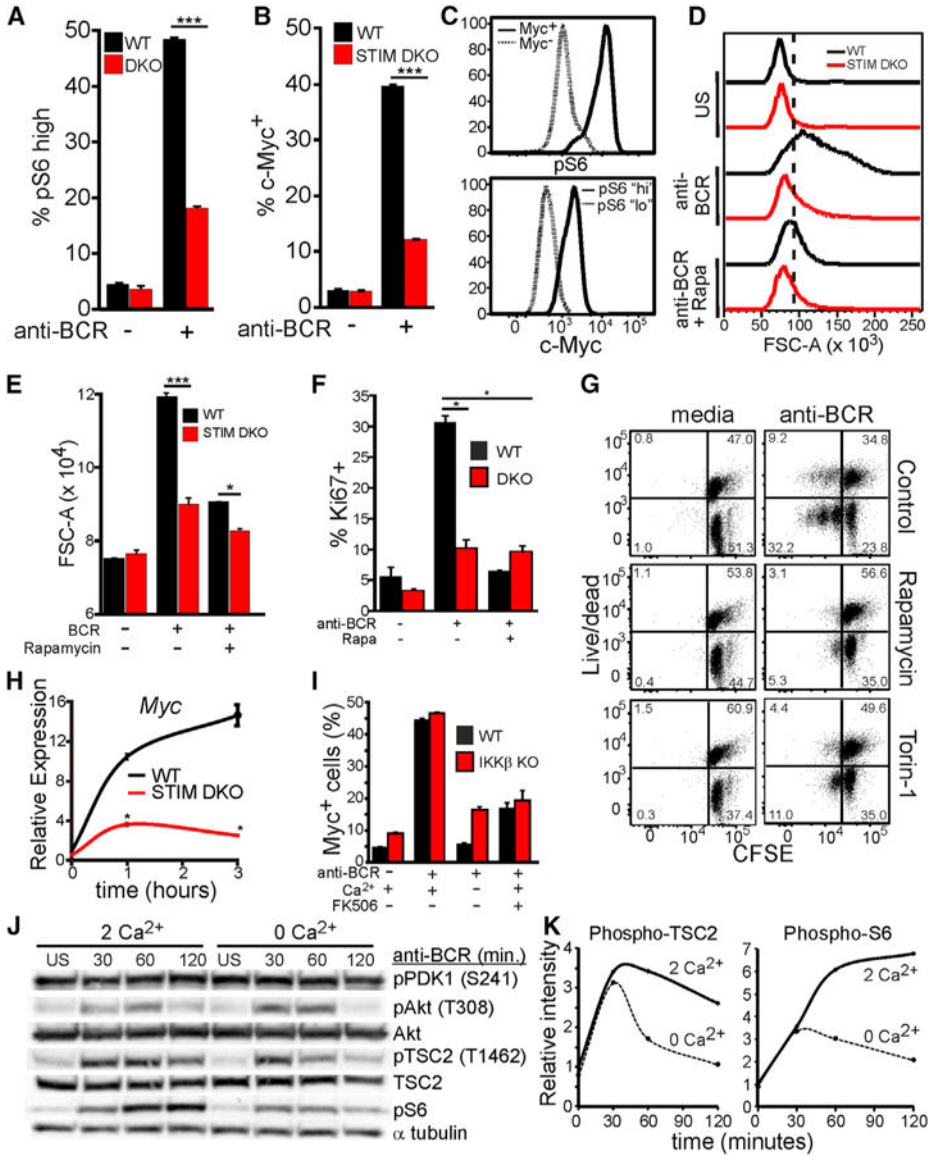

Figure 4. Ca^{2+} Is Required for mTORC1-and Myc-Dependent Cell-Cycle Entry

(A and B) Intracellular phosphorylated S6 (pS6) (A) and c-Myc protein expression (B) in WT and STIM DKO at 4 h of stimulation with anti-BCR (mean percentage ± SD from triplicate wells).

(C) pS6 expression in Myc^{+} and $Myc^{—}$ B cells (top, from B) and Myc expression in phospho-S6 ‘‘high’’ and phospho-S6 ‘‘low’’ populations (bottom, from A).

(D) Cell size (Forward scatter area or FSC-A) of anti-BCR-stimulated WT and STIM DKO B cells (32 h) and impact of the mTORC1 inhibitor rapamycin (25 nM).

(E) Cell size from (D) (mean FSC-A ± SD from triplicate wells).

(F) Ki67 expression (mean ± SD of triplicate wells) in WT and STIM DKO B cells following 32 h of anti-BCR and the impact of rapamycin (25 nM).

(G) CFSE dilution analysis of the proliferative dynamics of anti-BCR-stimulated WT B cells in the absence or presence of rapamycin (25 nM) or torin-1 (100 nM). Results are representative of triplicate measurements.

(H) Time course of *Myc* expression in $CD23^+$ B cells from WT (black line) and STIM DKO (red line) mice stimulated with anti-BCR (mean ± 95% confidence interval; *, statistically significant).

(I) c-Myc expression in $CD23^+$ B cells from $Ikk2^{fl/fl}$ 3 $Mb1cre^{—}$ (WT, black line) and $Ikk2^{fl/fl}$ 3 $Mb1cre^+$ (IKKβ KO, red line) mice stimulated with anti-BCR (6 h) in the absence or presence of FK506 (1 μM). Mean percentage of Myc^+ cells (±SD of triplicate measurements) is shown.

(j) Immunoblot of mTORC1 activity in B cells stimulated with anti-BCR in the presence and absence of extracellular Ca^{2+}.

(K) Densiometric analysis of phospho-TSC2-Thr1462 and phospho-S6 (from J). For all figures, *$p < 0.05$, **$p < 0.01$, ***$p < 0.001$.

See also Figure S3.

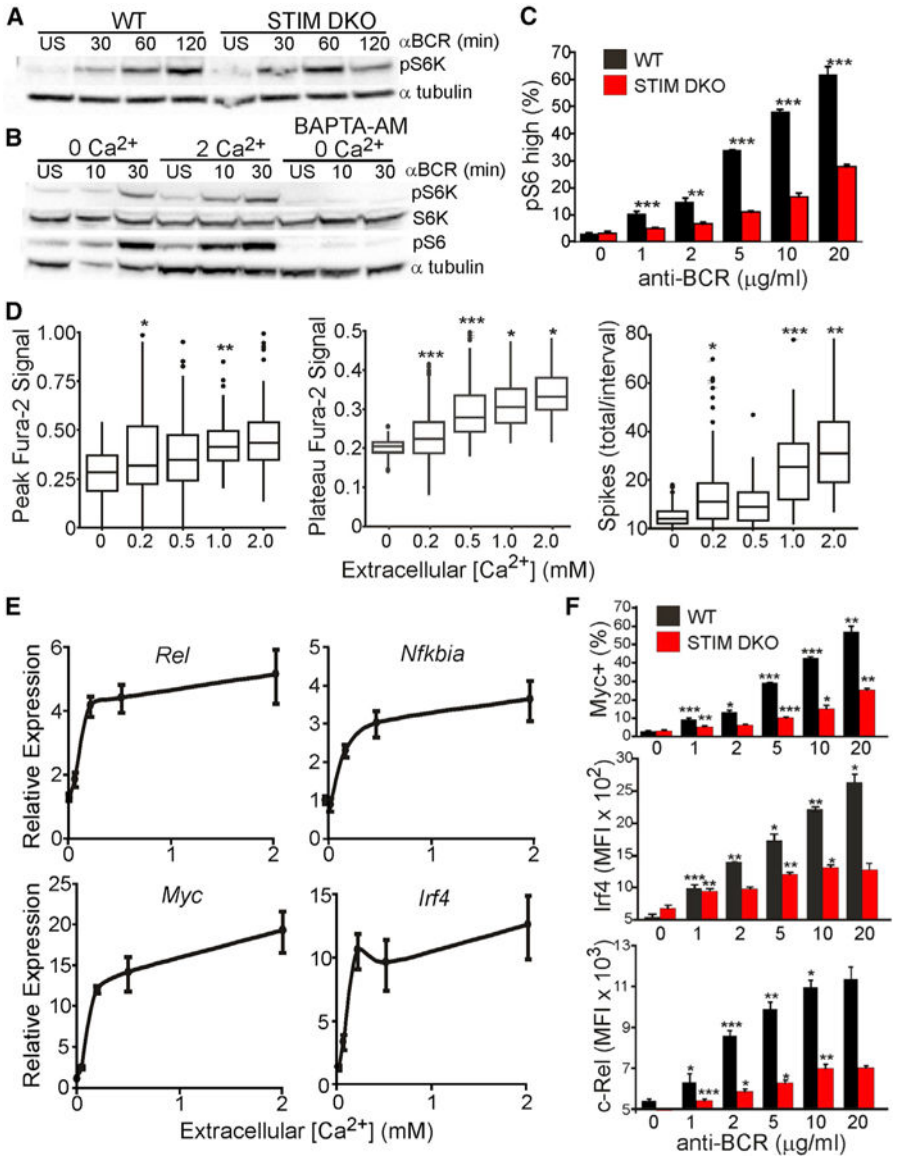

Figure 5. BCR-Induced Ca^{2+} Signals Tune mTORC1, NF-κB, and NFAT Activity

(A) Immunoblot analysis of S6 kinase phosphorylation (pS6K) in WT and STIM DKO B cells following stimulation with anti-BCR for times indicated.

(B) pS6K and S6 phosphorylation (pS6) following anti-BCR stimulation of WT B cells cultured in media containing 0 mM Ca^{2+} and 2 mM Ca^{2+} and in cells loaded with membrane-permeant Ca^{2+} chelator (BAPTA) in 0 mM Ca^{2+} medium.

(C) Anti-BCR dose dependence of pS6 in WT and STIM DKO at 6 h (mean percentage ± SD from triplicate wells are representative of two independent experiments).

(D) Boxplot representation of initial peak (left), average plateau/sustained concentration (from 10 to 15 min after anti-BCR, middle), and total Ca^{2+} spikes (20-min interval, right) in WT B cells stimulated in media containing indicated [Ca^{2+}]. Results are representative of three independent experiments with >50 cells per genotype and treatment.

(E) Extracellular Ca^{2+} dependence of *Rel*, *Nfkbia*, *Myc*, and *Irf4* mRNA expression 4 h after anti-BCR stimulation in media containing 0, 0.05, 0.2, 0.5, and 2.0 mM Ca^{2+} (mean ± 95% confidence interval; *, statistically significant).

(F) Anti-BCR dose-dependent expression of c-Myc, Irf4, and c-Rel protein in WT and STIM DKO at 6 h (mean percentage ± SD of triplicate measurements; representative of at least two independent experiments0.

For (C), (D), and (F), statistical significance was determined relative to preceding concentration of anti-BCR or extracellular [Ca^{2+}]. For all figures, *$p < 0.05$, **$p < 0.01$, ***$p < 0.001$.

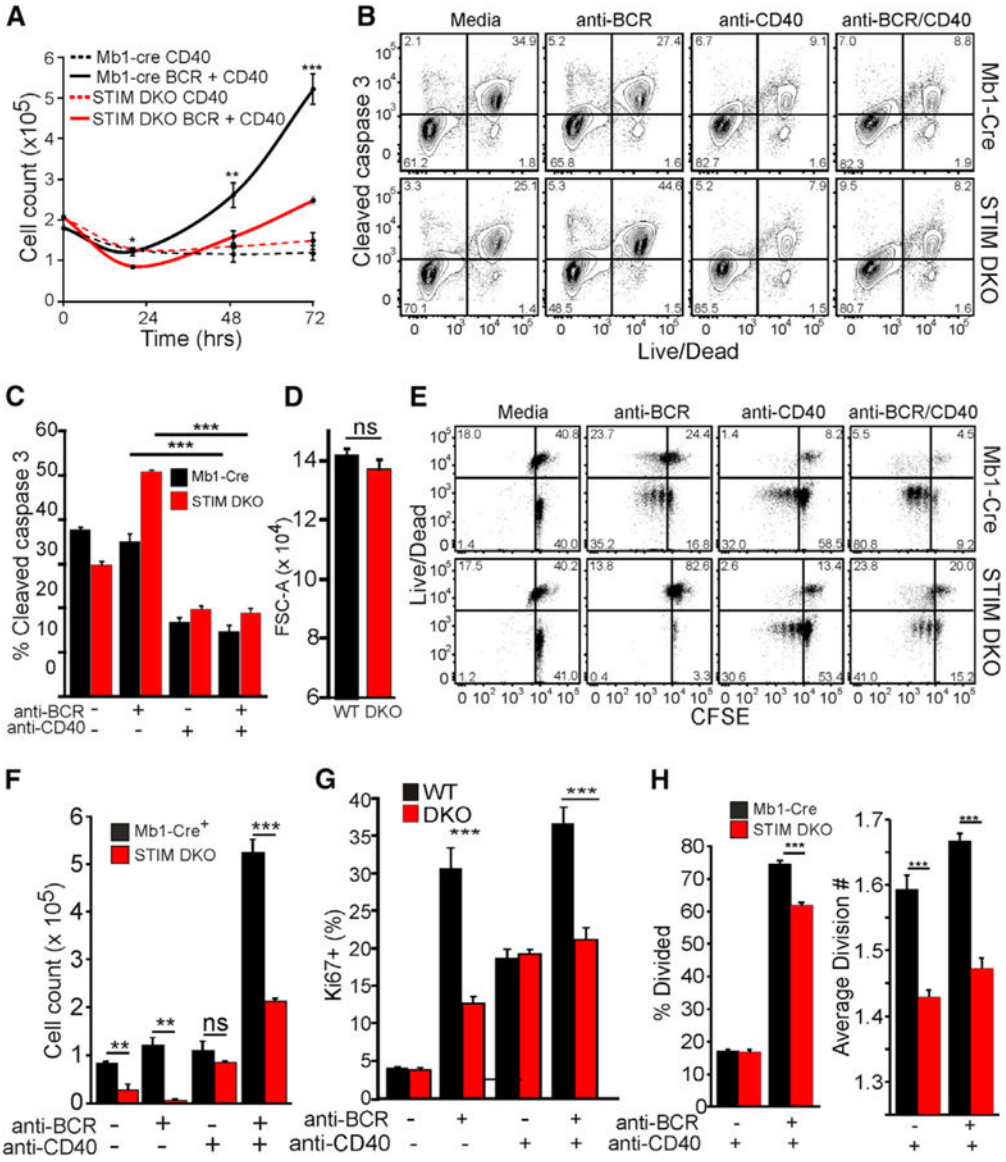

Figure 6. CD40 Costimulation Promotes B Cell Survival and Proliferation

(A) D23$^+$ B cells from WT (black) and STIM DKO (red) mice were cultured for indicated times in media containing anti-CD40 ± anti-BCR. The total number of live cells was enumerated, and mean cell numbers (±SD of triplicate wells) are plotted for the indicated time points.

(B) Intracellular cleaved caspase-3 in live and dead anti-BCR-stimulated WT and STIM DKO B cells (24 h).

(C) Frequency of cells containing cleaved caspase-3 from (B) (mean percentage ± SD of triplicate measurements).

(D) Cell size (FSC-A) analysis of WT and STIM DKO B cells stimulated with anti-BCR and anti-CD40 (results from triplicate wells and two independent experiments).

(E) CFSE dilution and live/dead analysis of WT and STIM DKO CD23$^+$ B cells stimulated as indicated for 72 h. Plots are representative of results from triplicate wells.

(F) Total live cells from (E) (mean ± SD from triplicate wells).
(G) Ki67 expression in WT and STIM DKO B cells following 32-h stimulation with anti-BCR in the absence or presence of anti-CD40 (mean percentage ± SD of $Ki67^+$ cells from triplicate wells from at least two independent experiments).
(H) Percentage of divided cells and mean division number for data shown in (E) (mean ± SD from triplicate wells).
For all figures, *$p < 0.05$, **$p < 0.01$, ***$p < 0.001$. See also Figure S4.

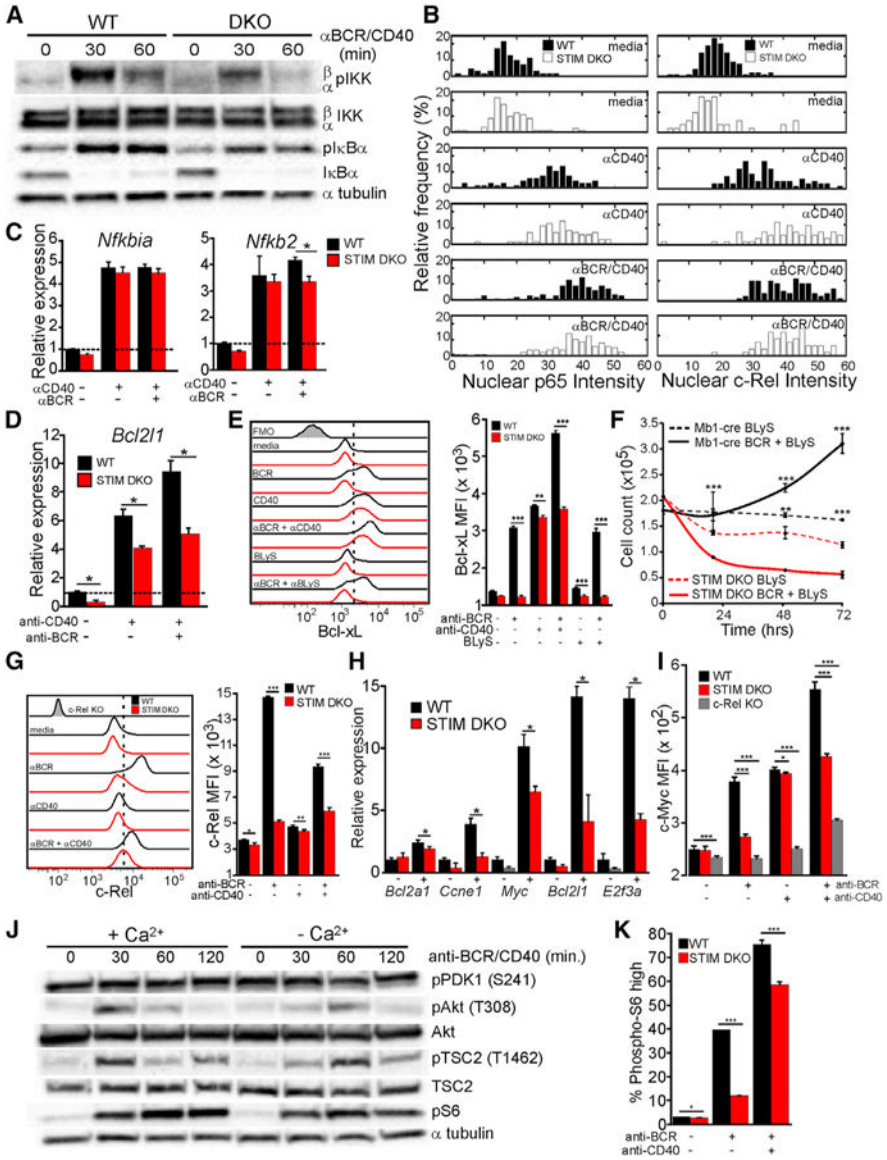

Figure 7. Ca^{2+}-Independent Activation of Canonical NF-κB and mTORC1 by CD40 Promotes B Cell Survival and Proliferation

(A) Immunoblot analysis of canonical NF-κB activation in $CD23^+$ WT and STIM DKO B cells stimulated with anti-BCR and anti-CD40 at indicated time points.

(B) NF-κB p65 (left) and c-Rel (right) nuclear intensity in WT (black) and STIM DKO (white) B cells (>70 cells per group) stimulated as indicated.

(C and D) (C) *Nfkbia* (IκBα) and *Nfkb2* (p100) and (D) *Bcl2l1* (Bcl-xL) mRNA expression in $CD23^+$ B cells from WT and STIM DKO mice stimulated for 3 h with anti-CD40 alone or anti-CD40 and anti-BCR (mean ± 95% confidence interval; *, statistically significant).

(E) Bcl-xL expression in WT (black line) and STIM DKO (red line) B cells after 6 h of anti-BCR in the absence or presence of BLyS (100 ng/mL) and the absence or presence of anti-CD40 (left) and plot of mean Bcl-xL MFI (±SD) from triplicate wells (right).

(F) Impact of BLyS (100 ng/mL) on the viability of unstimulated and anti-BCR-stimulated WT and STIM DKO B cells (mean cell number ± SD of triplicate wells).

(G) c-Rel expression in WT (black line) and STIM DKO (red line) B cells stimulated as indicated for 12 h. Average MFI (±SD) of triplicate wells (right) is shown.
(H) Expression of c-Rel target genes *Bcl2a1* (A1), *Ccne1* (Cyclin E), *Myc* (c-Myc), *Bcl2l1*, and *E2f3a* (E2f3) in WT (black) and STIM DKO B cells (red) 24 h following stimulation with anti-BCR and anti-CD40 (mean ± 95% confidence interval; *, statistically significant).
(I) c-Myc expression in WT (black line), STIM DKO (red line), and c-Rel KO (gray) B cells following 20 h of culture with no stimulus (media), anti-BCR, or anti-BCR/CD40.
(J) Immunoblot of mTORC1 activity in B cells stimulated with anti-BCR and anti-CD40 in Ca^{2+} containing (2 mM) or Ca^{2+}-free medium.
(K) Plot of phospho-S6 (pS6)-positive WT (black) and STIM DKO (red) B cells at 20 h of anti-BCR or anti-BCR/CD40 stimulation (mean percentage ± SD from triplicate wells). For all figures except where indicated, *$p < 0.05$, **$p < 0.01$, ***$p < 0.001$.

KEY RESOURCES TABLE

REAGENT or RESOURCE	SOURCE	IDENTIFIER
Antibodies		
anti-FoxO1 (C29H4) Rabbit mAb	Cell Signaling	Cat#2880S; RRID:AB_2106495
anti-c-Myc PE (D84C12)	Cell Signaling	Cat#14819 RRID:AB_2798629
S6 Ribosomal Protein (54D2) Mouse mAb	Cell Signaling	Cat#2317 RRID:AB_2238583
Phospho-Tuberin/TSC2 (Thr1462) Antibody	Cell Signaling	Cat#3611 RRID:AB_329855
Phospho-Akt (Thr308) (244F9) Rabbit mAb	Cell Signaling	Cat#4056 RRID:AB_331163
Phospho-Akt (Ser473) (D9E) XP® Rabbit mAb	Cell Signaling	Cat#4060S
Akt (pan) (C67E7) Rabbit mAb	Cell Signaling	Cat#4691 RRID:AB_915783
Phospho-PDK1 (Ser241) (C49H2) Rabbit mAb	Cell Signaling	Cat#3438 RRID:AB_2161134
Phospho-p70 S6 Kinase (Thr389) (108D2) Rabbit mAb	Cell Signaling	Cat#9234 RRID:AB_2269803
p70 S6 Kinase (49D7) Rabbit mAb	Cell Signaling	Cat#2708 RRID:AB_10694087
Cleaved Caspase-3 (Asp175) (5A1E) Rabbit mAb	Cell Signaling	Cat#9664 RRID:AB_2070042
Phospho-IKKα/β (Ser176/180) (16A6) Rabbit mAb	Cell Signaling	Cat#2697 RRID:AB_2079382
IKKβ (D30C6) Rabbit mAb	Cell Signaling	Cat#8943 RRID:AB_11024092
Phospho-IκBα (Ser32) (14D4) Rabbit mAb	Cell Signaling	Cat#2859 RRID:AB_561111
IκBα (L35A5) Mouse mAb (Amino-terminal Antigen) #4814	Cell Signaling	Cat#4814S RRID:AB_390781
anti-alpha-tubulin	Sigma Aldrich	Cat#T1568
anti-Ki67	Millipore Sigma	Cat#AB9260
Tuberin/TSC2 (D93F12) XP® Rabbit mAb	Cell Signaling	Cat#4308 RRID:AB_10547134
anti-phospho-S6 PE-Cy7 (D57.2.2E)	Cell Signaling	Cat#34411S RRID:AB_2799051
anti-c-Rel eF660 (1RELAH5)	Thermo Scientific	Cat#50–6111-80 RRID:AB_2574261
anti-c-Rel PE (REA397)	Miltenyi Biotec	Cat#130–124-715 RRID:AB_2651454
Anti-IRF-4-PE-Vio770	Miltenyi Biotec	Cat#130–100-909 RRID:AB_2652519
anti-Bcl-xL (54H6)	Cell Signaling	Cat# 2764S RRID:AB_2228008
Alex Fluor 488 goat anti-rabbit secondary antibody	Thermo Fisher	Cat#A11008 RRID:AB_143165
AffiniPure F(ab′)2 Fragment Goat Anti-Mouse IgM, Mu Chain Specific	Jackson ImmunoResearch	Cat#115–006-020 RRID:AB_2338469
LEAF Purified anti-mouse CD40 antibody (HM40–3)	BioLegend	Cat#102908 RRID:AB_312951
Purified anti-mouse CD16/32 Antibody	BioLegend	Cat#101302 RRID:AB_312801
Protein A HRP	Cell Signaling	Cat#12291
Goat anti-Rabbit IgG (H+L) Secondary Antibody, HRP	Thermo Fisher	Cat#65–6120 RRID:AB_2533967
Goat anti-Mouse IgG (H+L) Secondary Antibody, HRP	Thermo Fisher	Cat#62–6520 RRID:AB_88369
Chemicals, Peptides, and Recombinant Proteins		
CFSE	Biolegend	Cat#423801
Fura-2AM	Molecular Probes	CAS 108964–32-5
FK506 (tacrolimus)	Tocris Bioscience	Cat#3631/10
Cyclosporine A	Tocris Bioscience	Cat#1101
Torin-1	Tocris Bioscience	Cat#4247
Rapamycin (Sirolimus)	Selleck Chemical	Cat#S1039

REAGENT or RESOURCE	SOURCE	IDENTIFIER
W-7 hydrochloride	Tocris Bioscience	Cat#0369
Fluoromount G	Molecular Probes	CAS 108964–32-5
eBioscience Permeabilization Buffer (10X)	Thermo Fisher	Cat#00–8333-56
Paraformaldehyde Aqueous Solution —16%	Electron Microscopy Systems	CAS #30525–89-4
Corning Cell-Tak Cell and Tissue Adhesive	Fisher Scientific	Cat#CB40240
Hoechst 33342	Life Technologies	Cat#H3570
LIVE/DEAD Fixable Aqua Dead Cell Stain	Thermo Fisher	Cat#L34957
LIVE/DEAD Fixable eF780 Dead Cell Stain	Thermo Fisher	Cat#65–0865
Annexin V, FITC conjugate	Thermo Fisher	Cat#A13199
Critical Commercial Assays		
CD23 MicroBeads, mouse	Miltenyi Biotec	Cat#130–098-784
RNeasy Micro Kit	QIAGEN	Cat#74034
PERFECTA SYBR SMX L-ROX	VWR	Cat#101414–168
High-Capacity RNA-to-cDNA Kit	Applied Biosystems	Cat#4387406
AccuStart II GelTrack PCR SuperMix, QuantaBio	VWR	Cat#76047–140
Experimental Models: Organisms/Strains		
Mouse: Bcl-xL Tg: B6.Bcl2l1^{Tg} mice	Grillot et al., 1996	N/A
Mouse: Stim1$^{fl/fl}$Stim2$^{fl/fl}$: B6(Cg)-*Stim1*^{tm1Rao}/J *Stim2*^{tm1Rao}/J	Oh-Hora et al., 2008	N/A
Mouse: Mb1-cre(Stim1$^{fl/fl}$Stim2$^{fl/fl}$): B6(Cg)-*Stim1*^{tm1Rao}/J x*Stim2*^{tm1Rao}/J x B6.C(Cg)-*Cd79a*$^{tm1(cre)}$ *Reth*/EhobJ	This paper	N/A
Mouse: Ikk2$^{fl/fl}$	Greten et al., 2004	N/A
Mouse: Mb1-cre(Ikk2$^{fl/fl}$)	This paper	N/A
Mouse: C57BL/6J	Jackson Laboratory	N/A
Mouse: Ripk3$^{-/-}$Casp8$^{-/-}$	Oberst et al., 2011	N/A
Mouse: Mb1-cre+: B6.C(Cg)-*Cd79a*$^{tm1(cre)Reth}$/EhobJ	Hobeika et al., 2006	N/A
Mouse: Rel$^{-/-}$	Liou et al., 1999	N/A
Oligonucleotides		
qRT-PCR Primers	See Table S1 for all primers	N/A
Software and Algorithms		
ImageJ	ImageJ	https://imagej.net/ImageJ
Flow Jo_v9	Flow Jo	https://www.flowjo.com
Rstudio_v1.1.456	Rstudio	https://rstudio.com/
R_v3.5.1	R	https://www.r-project.org/
Bioconductor_v3.10	Bioconductor	https://www.bioconductor.org/install/
Matlab_R2017b	MATLAB	https://www.mathworks.com/products/matlab.html